Large-amplitude coupled scale-dependent behaviour of geometrically imperfect NSGT nanotubes

Ali Farajpour [a*], Mergen H. Ghayesh [a], Hamed Farokhi [b]

[a] *School of Mechanical Engineering, University of Adelaide, South Australia 5005, Australia*
Email: mergen.ghayesh@adelaide.edu.au (M.H. Ghayesh)
[*] *Corresponding author: ali.farajpourouderji@adelaide.edu.au (A. Farajpour)*

[b] *Department of Mechanical and Construction Engineering, Northumbria University, Newcastle upon Tyne NE1 8ST, UK*
Email: hamed.farokhi@northumbria.ac.uk (H. Farokhi)

Abstract

In this paper, a scale-dependent coupled nonlinear continuum-based model is developed for the mechanical behaviour of imperfect nanoscale tubes incorporating both the effect of the stress nonlocality and strain gradient effects. The scale effects on the nonlinear mechanics are taken into consideration employing a modified elasticity theory on the basis of a refined combination of Eringen's elasticity and the strain gradient theory. According to the Euler–Bernoulli theory of beams, the nonlocal strain gradient theory (NSGT) and Hamilton's principle, the potential energy, kinetic energy and the work performed by harmonic loads are formulated, and then the coupled scale-dependent equations of the imperfect nanotube are derived. Finally, Galerkin's scheme, as a discretisation technique, and the continuation method, as a solution procedure for ordinary differential equations, are used. The effects of geometrical imperfections in conjunction with other nanosystem parameters such as the nonlocal coefficient as well as the strain gradient coefficient on the coupled large-amplitude mechanical behaviour are explored and discussed.

Keywords: Nanotubes; Imperfections; Nonlinearity; Nonlocal effects; Strain gradient effects

1. Introduction

Nanostructures such as nanorings, nanotubes and nanosheets which form the fundamental building blocks of some nanoelectromechanical systems (NEMS) are scarcely a perfect structural element. During the fabrication process, a geometric imperfection is likely to be formed in the structure of nanomaterials since manufacturing at nanoscale levels is difficult to be implemented with high precision. Therefore, it is important to take these imperfections into account in a theoretical model or molecular dynamics (MD) simulations so as to obtain more accurate results.

In addition to experimental measurements and MD simulations, theoretical modelling of nanoscale structures has attracted researchers' attention in recent years due to its simplicity and low computational costs [1-7]. In addition to microscale structures [8-10], various size-dependent continuum-based models for nanoscale structures have been proposed [11-16]. For instance, Guo et al. [17] examined the influence of length scale on the mechanical response of nanoscale beams while moving in the axial direction and rotating; the critical velocity of rotation is greater for forward waves than that of backward waves. Li et al. [18] studied the influence of the nonlocality along the thickness of nanoscale beams; analytical expressions were proposed for the buckling behaviour. More recently, wave propagations in smart nanoscale tubes and shells have been investigated using a size-dependent continuum-based formulation [19]. Lei et al. [20] examined the size-dependent elasticity of cantilever small-scale beams carrying out experiments. In addition, in an interesting article, an experimental scheme was proposed by Li et al. [21] for obtaining the scale parameter of a size-dependent theory. Now previous studies related to the continuum-based modelling of size-dependent imperfect nanostructures are reviewed. Farshidianfar and Soltani [22] used

the nonlocal continuum mechanics to investigate the transverse dynamics of a geometrically imperfect fluid-conveying carbon nanotube (CNT) with both edges immovable; they obtained an approximate explicit expression for the nonlinear natural frequencies employing a multi-scale perturbation technique. Wang et al. [23] also developed a nonlocal beam model in order to examine the large-amplitude forced dynamics of imperfect single-walled CNTs; they utilised a one-term Galerkin approximation and the precise integration scheme to describe the nonlinear behaviour of the CNT. In another study, Mohammadi et al. [24] applied Eringen's elasticity theory to nanoscale beams with a geometrical imperfection resting on an elastic foundation so as to explore their post-buckling behaviour. In order to examine the stability response of metal foam nanoscale beams with an initial deflection in the presence of structural porosities, a nonlinear nonlocal analysis was also performed by Barati and Zenkour [25]. The effect of out-of-plane defects on the free dynamics of a single-layered graphene sheets was investigated by Jalali et al. [26] via use of Eringen's elasticity theory; they reported that out-of-plane defects have an important role to play in the free vibration of graphene sheets. Furthermore, Rafiee et al. [27] used the classical (local) continuum mechanics in conjunction with the first-order shear deformation theory in order to explore the large-amplitude dynamic instability of imperfect piezoelectric functionally graded (FG) plates reinforced by CNTs. A nonlocal beam model was also developed by Arefi and Salimi [28] to study the influence of the small initial curvature on the mechanical behaviour of single-walled CNTs. In addition, the effects of geometrical imperfections on the vibration response of graphene sheets [29] and on the large-amplitude instability of FG nanopanels [30] have been investigated. In addition, size influences have been studied on the nonlinear mechanics of microscale structures in recent years [31-33].

Recently, it has been reported that taking into account both the stress nonlocality and strain gradients leads to a more reliable size-dependent theoretical model for nanorods [34], nanobeams [35-37], functionally graded nanostructures [38, 39], protein microtubules [40] and graphene sheets [41]. However, all of the above-described valuable theoretical models of size-dependent imperfect nanoscale structures contain only one scale parameter (mainly only one nonlocal parameter) which is incapable of incorporating the size effect thoroughly. In the present study, for the first time, a nonlinear size-dependent nanobeam model is developed for imperfect nanotubes with consideration of both the stress nonlocality and strain gradients. The effect of being nanosized is incorporated into the modified continuum model within the framework of the nonlocal counterpart of the classical continuum mechanics as well as a strain gradient-based theory. The Euler–Bernoulli beam theory (EBBT), as a deformation model, is employed together with Hamilton's principle, as a work/energy law, for the derivation of the coupled scale-dependent equations of geometrically imperfect nanoscale tubes. The nonlinear mechanical behaviour of the imperfect nanosystem is obtained on the basis of Galerkin's scheme and a continuation-based approach. It is predicted that the present modified continuum-based model would be useful in design and manufacturing of NEMS devices using different nanotubes such as silver, carbon and silicon nanotubes.

2. Size-dependent formulation and solution technique

Figure 1 illustrates a nanoscale tube with a geometrical imperfection subject to external harmonic force. The geometrical imperfection is described by an arbitrary initial curvature as shown in the figure. The length and thickness of the nanotube are respectively denoted by L and h while the inner and outer radii are indicated by R_i and R_o, respectively. Moreover, the

area and the inertia moment of the cross-section of the tube are denoted by A and I, respectively. E, ρ and v also represent the elasticity modulus, the mass density and Poisson's ratio of the nanoscale tube, respectively.

According the EBBT, the nonlinear axial strain (ε_{xx}) of the geometrically imperfect nanoscale tube is obtained as

$$\varepsilon_{xx} = \frac{\partial u}{\partial x} + \frac{1}{2}\left(\frac{\partial w}{\partial x}\right)^2 + \frac{\partial w}{\partial x}\frac{dw_0}{dx} - z\frac{\partial^2 w}{\partial x^2}, \tag{1}$$

in which u, w and w_0 represent the longitudinal, transverse and initial transverse displacements of the imperfect nanosystem, respectively; x, z and t are the longitudinal coordinate, the transverse coordinate and the time, respectively. There are various size-dependent theories for nanoscale structures [42-46] as well as modified elasticity theories for microscale structures [47-49]. In this paper, the NSGT [38, 50, 51] is utilised for capturing size effects. The nonlocal strain gradient constitutive equation of the nanotube can be formulated as [52, 53]

$$t_{xx} - \left(e_0 a\right)^2 \nabla^2 t_{xx} = E\varepsilon_{xx} - El_{sg}^2 \nabla^2 \varepsilon_{xx}, \tag{2}$$

where t_{xx}, l_{sg} and $e_0 a$ are the total stress along the axial direction, the strain gradient parameter and the nonlocal parameter, respectively; ∇^2 indicates the Laplace operator; e_0 and a are a scale parameter for calibrating the theoretical model and the internal characteristics length of the nanotube, respectively [54, 55]. The strain gradient parameter and the nonlocal parameter are determined using experimental measurements or MD simulations [21, 56, 57]. For instance, Li et al. [35] obtained the scale parameters of carbon

nanotubes for the wave propagation analysis via MD simulations. Using Eqs. (1) and (2), one can derive the following relations

$$\left[1-\left(e_0a\right)^2\nabla^2\right]N_{xx}=EA\left(1-l_{sg}^2\nabla^2\right)\left[\frac{\partial u}{\partial x}+\frac{1}{2}\left(\frac{\partial w}{\partial x}\right)^2+\frac{\partial w}{\partial x}\frac{dw_0}{dx}\right], \tag{3a}$$

$$\left[1-\left(e_0a\right)^2\nabla^2\right]M_{xx}=-EI\left(1-l_{sg}^2\nabla^2\right)\frac{\partial^2 w}{\partial x^2}, \tag{3b}$$

with N_{xx} being the longitudinal force resultant and M_{xx} being the bending couple resultant, which are defined by

$$\begin{Bmatrix}N_{xx}\\M_{xx}\end{Bmatrix}=\int_A\begin{Bmatrix}1\\z\end{Bmatrix}t_{xx}dA. \tag{4}$$

Applying the nonlocal strain gradient theory (NSGT) to the imperfect nanoscale tube, the variation of the elastic energy is obtained as

$$\delta U=\int_0^L\int_A\left(\sigma_{xx}\delta\varepsilon_{xx}+\sigma_{xx}^{(1)}\nabla\delta\varepsilon_{xx}\right)dAdx=\int_0^L\int_A t_{xx}\delta\varepsilon_{xx}dAdx+\left[\int_A\sigma_{xx}^{(1)}\delta\varepsilon_{xx}dA\right]_0^L, \tag{5}$$

in which σ_{xx} and $\sigma_{xx}^{(1)}$ are respectively the traditional nonlocal axial stress and the higher-order nonlocal axial stress, and ∇ represents the gradient operator; *U* stands for the elastic energy of the nanotube. It should be noted that the relation between the various stress components is given by $t_{xx}=\sigma_{xx}-\nabla\sigma_{xx}^{(1)}$ on the basis of the NSGT. Consider a nanoscale tube of mass per unit length *m* subject to the harmonic transverse loading $F\left(x\right)\cos\left(\omega t\right)$ in which *F* and ω represent the force amplitude and frequency, respectively. The corresponding motion and work variations can be written as

$$\delta K=m\int_0^L\left(\frac{\partial u}{\partial t}\delta\frac{\partial u}{\partial t}+\frac{\partial w}{\partial t}\delta\frac{\partial w}{\partial t}\right)dx, \tag{6a}$$

$$\delta W_F=\int_0^L F\left(x\right)\cos\left(\omega t\right)\delta w\,\mathrm{d}x. \tag{6b}$$

Here K and W_F are the motion energy and the external work associated with the transverse harmonic force, respectively. To derive the differential equations of motion, the following steps are taken:

1) Substituting Eqs. (5) and (6) into $\int_{t_1}^{t_2}\left(\delta K+\delta W_F-\delta U\right)\mathrm{d}t=0$ (i.e. Hamilton's principle).

2) Integrating by parts and collecting the coefficient of δu and δw.

The resultant differential equations of motion are as

$$\frac{\partial N_{xx}}{\partial x}=m\frac{\partial^2 u}{\partial t^2}, \tag{7a}$$

$$\frac{\partial^2 M_{xx}}{\partial x^2}+\frac{\partial}{\partial x}\left[N_{xx}\left(\frac{\partial w}{\partial x}+\frac{dw_0}{dx}\right)\right]=m\frac{\partial^2 w}{\partial t^2}-F(x)\cos(\omega t). \tag{7b}$$

The related boundary conditions are also obtained as

$$N_{xx}=0 \text{ or } u=0,\ N_{xx}\left(\frac{\partial w}{\partial x}+\frac{dw_0}{dx}\right)+\frac{\partial M_{xx}}{\partial x}=0 \text{ or } w=0,\ M_{xx}=0 \text{ or } \frac{\partial w}{\partial x}=0, \tag{8a}$$

$$N_{xx}^{(1)}=0 \text{ or } \frac{\partial u}{\partial x}=0,\ N_{xx}^{(1)}\left(\frac{\partial w}{\partial x}+\frac{dw_0}{dx}\right)=0 \text{ or } \frac{\partial w}{\partial x}=0,\ M_{xx}^{(1)}=0 \text{ or } \frac{\partial^2 w}{\partial x^2}=0, \tag{8b}$$

where

$$\begin{Bmatrix} N_{xx}^{(1)} \\ M_{xx}^{(1)} \end{Bmatrix}=\int_A \begin{Bmatrix} 1 \\ z \end{Bmatrix}\sigma_{xx}^{(1)}dA. \tag{9}$$

Using the relations of stress resultants (i.e. Eq. (3)) and the above differential equations (i.e. Eq. (7)), the following explicit relations are obtained

$$N_{xx}=EA\left(1-l_{sg}^2\nabla^2\right)\left[\frac{\partial u}{\partial x}+\frac{1}{2}\left(\frac{\partial w}{\partial x}\right)^2+\frac{\partial w}{\partial x}\frac{dw_0}{dx}\right]+m\left(e_0a\right)^2\frac{\partial^3 u}{\partial x\partial t^2}, \tag{10a}$$

$$\begin{aligned} M_{xx}=&-EI\left(1-l_{sg}^2\nabla^2\right)\frac{\partial^2 w}{\partial x^2}+m\left(e_0a\right)^2\frac{\partial^2 w}{\partial t^2}\\ &-\left(e_0a\right)^2F(x)\cos(\omega t)-\left(e_0a\right)^2\frac{\partial}{\partial x}\left[N_{xx}\left(\frac{\partial w}{\partial x}+\frac{dw_0}{dx}\right)\right]. \end{aligned} \tag{10b}$$

Substituting Eq. (10) into Eq. (7) leads to the following NSGT-based coupled nonlinear equations for the geometrically imperfect nanoscale tube

$$EA\left[\frac{\partial^2 u}{\partial x^2}+\frac{\partial w}{\partial x}\frac{\partial^2 w}{\partial x^2}+\frac{\partial^2 w}{\partial x^2}\frac{dw_0}{dx}+\frac{\partial w}{\partial x}\frac{d^2 w_0}{dx^2}-l_{sg}^2\left(\frac{\partial^4 u}{\partial x^4}+3\frac{\partial^2 w}{\partial x^2}\frac{\partial^3 w}{\partial x^3}+\frac{\partial w}{\partial x}\frac{\partial^4 w}{\partial x^4}\right.\right.$$
$$\left.\left.+\frac{\partial^4 w}{\partial x^4}\frac{dw_0}{dx}+3\frac{\partial^3 w}{\partial x^3}\frac{d^2 w_0}{dx^2}+3\frac{\partial^2 w}{\partial x^2}\frac{d^3 w_0}{dx^3}+\frac{\partial w}{\partial x}\frac{d^4 w_0}{dx^4}\right)\right]=m\frac{\partial^2 u}{\partial t^2}-m\left(e_0 a\right)^2\frac{\partial^4 u}{\partial x^2\partial t^2}, \tag{11}$$

$$EI\left(l_{sg}^2\frac{\partial^6 w}{\partial x^6}-\frac{\partial^4 w}{\partial x^4}\right)+EA\left[\frac{\partial^2 w}{\partial x^2}+\frac{d^2 w_0}{dx^2}-\left(e_0 a\right)^2\left(\frac{\partial^4 w}{\partial x^4}+\frac{d^4 w_0}{dx^4}\right)\right]\left[\frac{\partial u}{\partial x}+\frac{1}{2}\left(\frac{\partial w}{\partial x}\right)^2+\frac{\partial w}{\partial x}\frac{dw_0}{dx}\right]$$
$$+EA\left[\frac{\partial w}{\partial x}+\frac{dw_0}{dx}-3\left(e_0 a\right)^2\left(\frac{\partial^3 w}{\partial x^3}+\frac{d^3 w_0}{dx^3}\right)\right]\left(\frac{\partial^2 u}{\partial x^2}+\frac{\partial w}{\partial x}\frac{\partial^2 w}{\partial x^2}+\frac{\partial^2 w}{\partial x^2}\frac{dw_0}{dx}+\frac{\partial w}{\partial x}\frac{d^2 w_0}{dx^2}\right)$$
$$-EA\left\{\left[l_{sg}^2+3\left(e_0 a\right)^2\right]\left(\frac{\partial^2 w}{\partial x^2}+\frac{d^2 w_0}{dx^2}\right)-\left(e_0 a\right)^2 l_{sg}^2\left(\frac{\partial^4 w}{\partial x^4}+\frac{d^4 w_0}{dx^4}\right)\right\}\times$$
$$\left[\frac{\partial^3 u}{\partial x^3}+\left(\frac{\partial^2 w}{\partial x^2}\right)^2+\frac{\partial w}{\partial x}\frac{\partial^3 w}{\partial x^3}+\frac{\partial^3 w}{\partial x^3}\frac{dw_0}{dx}+2\frac{\partial^2 w}{\partial x^2}\frac{d^2 w_0}{dx^2}+\frac{\partial w}{\partial x}\frac{d^3 w_0}{dx^3}\right]$$
$$-EA\left\{\left[l_{sg}^2+\left(e_0 a\right)^2\right]\left(\frac{\partial w}{\partial x}+\frac{dw_0}{dx}\right)-3\left(e_0 a\right)^2 l_{sg}^2\left(\frac{\partial^3 w}{\partial x^3}+\frac{d^3 w_0}{dx^3}\right)\right\}\times$$
$$\left(\frac{\partial^4 u}{\partial x^4}+3\frac{\partial^2 w}{\partial x^2}\frac{\partial^3 w}{\partial x^3}+\frac{\partial w}{\partial x}\frac{\partial^4 w}{\partial x^4}+\frac{\partial^4 w}{\partial x^4}\frac{dw_0}{dx}+3\frac{\partial^3 w}{\partial x^3}\frac{d^2 w_0}{dx^2}+3\frac{\partial^2 w}{\partial x^2}\frac{d^3 w_0}{dx^3}+\frac{\partial w}{\partial x}\frac{d^4 w_0}{dx^4}\right)$$
$$+3EAl_{sg}^2\left(e_0 a\right)^2\left(\frac{\partial^2 w}{\partial x^2}+\frac{d^2 w_0}{dx^2}\right)\left[\frac{\partial^5 u}{\partial x^5}+3\left(\frac{\partial^3 w}{\partial x^3}\right)^2+4\frac{\partial^2 w}{\partial x^2}\frac{\partial^4 w}{\partial x^4}+\frac{\partial w}{\partial x}\frac{\partial^5 w}{\partial x^5}+\frac{\partial^5 w}{\partial x^5}\frac{dw_0}{dx}\right.$$
$$\left.+4\frac{\partial^4 w}{\partial x^4}\frac{d^2 w_0}{dx^2}+6\frac{\partial^3 w}{\partial x^3}\frac{d^3 w_0}{dx^3}+4\frac{\partial^2 w}{\partial x^2}\frac{d^4 w_0}{dx^4}+\frac{\partial w}{\partial x}\frac{d^5 w_0}{dx^5}\right]$$
$$+EAl_{sg}^2\left(e_0 a\right)^2\left(\frac{\partial w}{\partial x}+\frac{dw_0}{dx}\right)\left(\frac{\partial^6 u}{\partial x^6}+10\frac{\partial^3 w}{\partial x^3}\frac{\partial^4 w}{\partial x^4}+5\frac{\partial^2 w}{\partial x^2}\frac{\partial^5 w}{\partial x^5}+\frac{\partial w}{\partial x}\frac{\partial^6 w}{\partial x^6}\right.$$
$$\left.+\frac{\partial^6 w}{\partial x^6}\frac{dw_0}{dx}+5\frac{\partial^5 w}{\partial x^5}\frac{d^2 w_0}{dx^2}+10\frac{\partial^4 w}{\partial x^4}\frac{d^3 w_0}{dx^3}+10\frac{\partial^3 w}{\partial x^3}\frac{d^4 w_0}{dx^4}+5\frac{\partial^2 w}{\partial x^2}\frac{d^5 w_0}{dx^5}+\frac{\partial w}{\partial x}\frac{d^6 w_0}{dx^6}\right)$$
$$-m\left(e_0 a\right)^2\left(\frac{\partial w}{\partial x}+\frac{dw_0}{dx}\right)\left[\left(e_0 a\right)^2\frac{\partial^6 u}{\partial x^4\partial t^2}-\frac{\partial^4 u}{\partial x^2\partial t^2}\right]-3m\left(e_0 a\right)^4\left(\frac{\partial^3 w}{\partial x^3}+\frac{d^3 w_0}{dx^3}\right)\frac{\partial^4 u}{\partial x^2\partial t^2}$$
$$-m\left(e_0 a\right)^2\left(\frac{\partial^2 w}{\partial x^2}+\frac{d^2 w_0}{dx^2}\right)\left[3\left(e_0 a\right)^2\frac{\partial^5 u}{\partial x^3\partial t^2}-\frac{\partial^3 u}{\partial x\partial t^2}\right]-m\left(e_0 a\right)^4\left(\frac{\partial^4 w}{\partial x^4}+\frac{d^4 w_0}{dx^4}\right)\frac{\partial^3 u}{\partial x\partial t^2} \tag{12}$$
$$=m\frac{\partial^2 w}{\partial t^2}-m\left(e_0 a\right)^2\frac{\partial^4 w}{\partial x^2\partial t^2}-F\left(x\right)\cos\left(\omega t\right)+\left(e_0 a\right)^2\frac{\partial^2}{\partial x^2}\left[F\left(x\right)\cos\left(\omega t\right)\right].$$

Assuming the amplitude of the harmonic loading as $F\left(x\right)=F_1$, and applying the following non-dimensional parameters to Eqs. (11) and (12)

$$x^* = \frac{x}{L},\ u^* = \frac{u}{r},\ w^* = \frac{w}{r},\ w_0^* = \frac{w_0}{r},\ \chi_{nl} = \frac{e_0 a}{L},\ \chi_{sg} = \frac{l_{sg}}{L},$$
$$\beta = \frac{L}{r},\ r = \sqrt{\frac{I}{A}},\ F_1^* = \frac{F_1 L^3}{EI},\ t^* = \frac{t}{L^2}\sqrt{\frac{EI}{m}},\ \Omega = \sqrt{\frac{L^4 m}{EI}}\omega, \tag{13}$$

one can obtain the non-dimensional equations of motions as

$$\beta\left[\beta\frac{\partial^2 u}{\partial x^2} + \frac{\partial w}{\partial x}\frac{\partial^2 w}{\partial x^2} + \frac{\partial^2 w}{\partial x^2}\frac{dw_0}{dx} + \frac{\partial w}{\partial x}\frac{d^2 w_0}{dx^2} - \chi_{sg}^2\left(\beta\frac{\partial^4 u}{\partial x^4} + 3\frac{\partial^2 w}{\partial x^2}\frac{\partial^3 w}{\partial x^3} + \frac{\partial w}{\partial x}\frac{\partial^4 w}{\partial x^4}\right.\right.$$
$$\left.\left. + \frac{\partial^4 w}{\partial x^4}\frac{dw_0}{dx} + 3\frac{\partial^3 w}{\partial x^3}\frac{d^2 w_0}{dx^2} + 3\frac{\partial^2 w}{\partial x^2}\frac{d^3 w_0}{dx^3} + \frac{\partial w}{\partial x}\frac{d^4 w_0}{dx^4}\right)\right] = \frac{\partial^2 u}{\partial t^2} - \chi_{nl}^2\frac{\partial^4 u}{\partial x^2 \partial t^2}, \tag{14}$$

$$\chi_{sg}^2\frac{\partial^6 w}{\partial x^6} - \frac{\partial^4 w}{\partial x^4} + \left[\frac{\partial^2 w}{\partial x^2} + \frac{d^2 w_0}{dx^2} - \chi_{nl}^2\left(\frac{\partial^4 w}{\partial x^4} + \frac{d^4 w_0}{dx^4}\right)\right]\left[\beta\frac{\partial u}{\partial x} + \frac{1}{2}\left(\frac{\partial w}{\partial x}\right)^2 + \frac{\partial w}{\partial x}\frac{dw_0}{dx}\right]$$
$$+\left[\frac{\partial w}{\partial x} + \frac{dw_0}{dx} - 3\chi_{nl}^2\left(\frac{\partial^3 w}{\partial x^3} + \frac{d^3 w_0}{dx^3}\right)\right]\left(\beta\frac{\partial^2 u}{\partial x^2} + \frac{\partial w}{\partial x}\frac{\partial^2 w}{\partial x^2} + \frac{\partial^2 w}{\partial x^2}\frac{dw_0}{dx} + \frac{\partial w}{\partial x}\frac{d^2 w_0}{dx^2}\right)$$
$$-\left[\left(\chi_{sg}^2 + 3\chi_{nl}^2\right)\left(\frac{\partial^2 w}{\partial x^2} + \frac{d^2 w_0}{dx^2}\right) - \chi_{nl}^2\chi_{sg}^2\left(\frac{\partial^4 w}{\partial x^4} + \frac{d^4 w_0}{dx^4}\right)\right]\times$$
$$\left[\beta\frac{\partial^3 u}{\partial x^3} + \left(\frac{\partial^2 w}{\partial x^2}\right)^2 + \frac{\partial w}{\partial x}\frac{\partial^3 w}{\partial x^3} + \frac{\partial^3 w}{\partial x^3}\frac{dw_0}{dx} + 2\frac{\partial^2 w}{\partial x^2}\frac{d^2 w_0}{dx^2} + \frac{\partial w}{\partial x}\frac{d^3 w_0}{dx^3}\right]$$
$$-\left[\left(\chi_{sg}^2 + \chi_{nl}^2\right)\left(\frac{\partial w}{\partial x} + \frac{dw_0}{dx}\right) - 3\chi_{nl}^2\chi_{sg}^2\left(\frac{\partial^3 w}{\partial x^3} + \frac{d^3 w_0}{dx^3}\right)\right]\left(\beta\frac{\partial^4 u}{\partial x^4} + 3\frac{\partial^2 w}{\partial x^2}\frac{\partial^3 w}{\partial x^3}\right.$$
$$\left. + \frac{\partial w}{\partial x}\frac{\partial^4 w}{\partial x^4} + \frac{\partial^4 w}{\partial x^4}\frac{dw_0}{dx} + 3\frac{\partial^3 w}{\partial x^3}\frac{d^2 w_0}{dx^2} + 3\frac{\partial^2 w}{\partial x^2}\frac{d^3 w_0}{dx^3} + \frac{\partial w}{\partial x}\frac{d^4 w_0}{dx^4}\right)$$
$$+3\chi_{nl}^2\chi_{sg}^2\left(\frac{\partial^2 w}{\partial x^2} + \frac{d^2 w_0}{dx^2}\right)\left[\beta\frac{\partial^5 u}{\partial x^5} + 3\left(\frac{\partial^3 w}{\partial x^3}\right)^2 + 4\frac{\partial^2 w}{\partial x^2}\frac{\partial^4 w}{\partial x^4} + \frac{\partial w}{\partial x}\frac{\partial^5 w}{\partial x^5} + \frac{\partial^5 w}{\partial x^5}\frac{dw_0}{dx}\right.$$
$$\left. + 4\frac{\partial^4 w}{\partial x^4}\frac{d^2 w_0}{dx^2} + 6\frac{\partial^3 w}{\partial x^3}\frac{d^3 w_0}{dx^3} + 4\frac{\partial^2 w}{\partial x^2}\frac{d^4 w_0}{dx^4} + \frac{\partial w}{\partial x}\frac{d^5 w_0}{dx^5}\right]$$
$$+\chi_{nl}^2\chi_{sg}^2\left(\frac{\partial w}{\partial x} + \frac{dw_0}{dx}\right)\left(\beta\frac{\partial^6 u}{\partial x^6} + 10\frac{\partial^3 w}{\partial x^3}\frac{\partial^4 w}{\partial x^4} + 5\frac{\partial^2 w}{\partial x^2}\frac{\partial^5 w}{\partial x^5} + \frac{\partial w}{\partial x}\frac{\partial^6 w}{\partial x^6} + \frac{\partial^6 w}{\partial x^6}\frac{dw_0}{dx}\right.$$
$$\left. + 5\frac{\partial^5 w}{\partial x^5}\frac{d^2 w_0}{dx^2} + 10\frac{\partial^4 w}{\partial x^4}\frac{d^3 w_0}{dx^3} + 10\frac{\partial^3 w}{\partial x^3}\frac{d^4 w_0}{dx^4} + 5\frac{\partial^2 w}{\partial x^2}\frac{d^5 w_0}{dx^5} + \frac{\partial w}{\partial x}\frac{d^6 w_0}{dx^6}\right)$$

$$-\frac{\chi_{nl}^2}{\beta}\left(\frac{\partial w}{\partial x}+\frac{dw_0}{dx}\right)\left(\chi_{nl}^2\frac{\partial^6 u}{\partial x^4\partial t^2}-\frac{\partial^4 u}{\partial x^2\partial t^2}\right)-3\frac{\chi_{nl}^4}{\beta}\left(\frac{\partial^3 w}{\partial x^3}+\frac{d^3w_0}{dx^3}\right)\frac{\partial^4 u}{\partial x^2\partial t^2}$$
$$-\frac{\chi_{nl}^2}{\beta}\left(\frac{\partial^2 w}{\partial x^2}+\frac{d^2w_0}{dx^2}\right)\left(3\chi_{nl}^2\frac{\partial^5 u}{\partial x^3\partial t^2}-\frac{\partial^3 u}{\partial x\partial t^2}\right)-\frac{\chi_{nl}^4}{\beta}\left(\frac{\partial^4 w}{\partial x^4}+\frac{d^4w_0}{dx^4}\right)\frac{\partial^3 u}{\partial x\partial t^2} \tag{15}$$
$$=\frac{\partial^2 w}{\partial t^2}-\chi_{nl}^2\frac{\partial^4 w}{\partial x^2\partial t^2}-F_1\,\beta\cos(\Omega t).$$

Here asterisk superscripts are neglected for convenience purposes. β, r, χ_{nl} and χ_{sg} stand for the slenderness ratio, the gyration radius, the nonlocal coefficient and the strain gradient coefficient, respectively. Furthermore, Ω represents the non-dimensional harmonic excitation frequency. In order to obtain a numerical solution for Eqs. (14) and (15), first Galerkin's procedure [58-61] as a discretisation method is utilised. In this way, the longitudinal and transverse displacements are as

$$u(x,t)=\sum_{j=1}^{N_x} r_j(t)\hat{u}_j(x), \tag{16a}$$

$$w(x,t)=\sum_{j=1}^{N_z} q_j(t)\hat{w}_j(x), \tag{16b}$$

where N_x and N_z denote the number of shape functions along the x and z axes, respectively; r_j and $\hat{u}_j$ represent the axial generalized coordinate and the axial shape function of the imperfect nanotube; also, q_j and $\hat{w}_j$ stand for the transverse generalized coordinate and the transverse shape function, respectively. Let us consider a geometric imperfection as $w_0=A_0\hat{w}_1(x)$ for the nanotube; A_0 indicates the imperfection amplitude. Assuming clamped-clamped (C-C) boundary conditions for the tube, the appropriate shape functions are

$$\begin{Bmatrix}\hat{w}_j(x)\\ \hat{u}_j(x)\end{Bmatrix}=\begin{Bmatrix}-\left[\frac{\cosh\lambda_j-\cos\lambda_j}{\sinh\lambda_j-\sin\lambda_j}\right]\left[\sinh(\lambda_j x)-\sin(\lambda_j x)\right]+\cosh(\lambda_j x)-\cos(\lambda_j x)\\ \sin(j\pi x)\end{Bmatrix}, \tag{17}$$

in which λ_j stand for the *j*th root of the classical frequency equation for C-C beams. It is worth mentioning that $\hat{w}_1(x)$ is obtained from Eq. (17) when *j* is set to 1. Inserting Eq. (16) into Eqs. (14) and (15) and then applying the Galerkin discretisation technique, one obtains

$$
\begin{aligned}
&\beta^2\sum_{j=1}^{N_x} r_j\left(\int_0^1 \hat{u}_k\hat{u}_j''dx\right)+\beta\sum_{j=1}^{N_z}\sum_{i=1}^{N_z} q_iq_j\left(\int_0^1 \hat{u}_k\hat{w}_i''\hat{w}_j'dx\right)+\beta A_0\sum_{j=1}^{N_z} q_j\left(\int_0^1 \hat{u}_k\hat{w}_j''\hat{w}_1'dx\right)\\
&+\beta A_0\sum_{j=1}^{N_z} q_j\left(\int_0^1 \hat{u}_k\hat{w}_j'\hat{w}_1''dx\right)-\beta\chi_{sg}^2\left[\beta\sum_{j=1}^{N_x} r_j\left(\int_0^1 \hat{u}_k\hat{u}_j''''dx\right)+3\sum_{i=1}^{N_z}\sum_{j=1}^{N_z} q_iq_j\left(\int_0^1 \hat{u}_k\hat{w}_i''\hat{w}_j'''dx\right)\right.\\
&+\sum_{j=1}^{N_z}\sum_{i=1}^{N_z} q_iq_j\left(\int_0^1 \hat{u}_k\hat{w}_i'\hat{w}_j''''dx\right)+A_0\sum_{j=1}^{N_z} q_j\left(\int_0^1 \hat{u}_k\hat{w}_j''''\hat{w}_1'dx\right)+3A_0\sum_{j=1}^{N_z} q_j\left(\int_0^1 \hat{u}_k\hat{w}_j'''\hat{w}_1''dx\right)\\
&\left.+3A_0\sum_{j=1}^{N_z} q_j\left(\int_0^1 \hat{u}_k\hat{w}_j''\hat{w}_1'''dx\right)+A_0\sum_{j=1}^{N_z} q_j\left(\int_0^1 \hat{u}_k\hat{w}_j'\hat{w}_1''''dx\right)\right]\\
&=\sum_{j=1}^{N_x}\ddot{r}_j\left(\int_0^1 \hat{u}_k\hat{u}_jdx\right)-\chi_{nl}^2\sum_{j=1}^{N_x}\ddot{r}_j\left(\int_0^1 \hat{u}_k\hat{u}_j''dx\right)\quad \text{for}\quad k=1,2,\cdots N_x,
\end{aligned}
\tag{18}
$$

$$
\begin{aligned}
&\int_0^1\hat{w}_k\left[\chi_{sg}^2\sum_{j=1}^{N_z} q_j\hat{w}_j^{(6)}-\sum_{j=1}^{N_z} q_j\hat{w}_j''''\right]dx\\
&+\int_0^1\left\{\hat{w}_k\left[\sum_{j=1}^{N_z} q_j\hat{w}_j''+A_0\hat{w}_1''-\chi_{nl}^2\left(\sum_{j=1}^{N_z} q_j\hat{w}_j''''+A_0\hat{w}_1''''\right)\right]\right.\\
&\left.\times\left[\beta\sum_{j=1}^{N_x} r_j\hat{u}_j'+\frac{1}{2}\sum_{i=1}^{N_z}\sum_{j=1}^{N_z} q_iq_j\hat{w}_i'\hat{w}_j'+A_0\sum_{j=1}^{N_z} q_j\hat{w}_j'\hat{w}_1'\right]dx\right\}\\
&+\int_0^1\left\{\hat{w}_k\left[\sum_{j=1}^{N_z} q_j\hat{w}_j'+A_0\hat{w}_1'-3\chi_{nl}^2\left(\sum_{j=1}^{N_z} q_j\hat{w}_j'''+A_0\hat{w}_1'''\right)\right]\right.\\
&\left.\times\left(\beta\sum_{j=1}^{N_x} r_j\hat{u}_j''+\sum_{i=1}^{N_z}\sum_{j=1}^{N_z} q_iq_j\hat{w}_j''\hat{w}_i'+A_0\sum_{j=1}^{N_z} q_j\left(\hat{w}_1'\hat{w}_j''+\hat{w}_1''\hat{w}_j'\right)\right)dx\right\}\\
&-\int_0^1\left\{\hat{w}_k\left[\left(\chi_{sg}^2+3\chi_{nl}^2\right)\left(\sum_{j=1}^{N_z} q_j\hat{w}_j''+A_0\hat{w}_1''\right)-\chi_{nl}^2\chi_{sg}^2\left(\sum_{j=1}^{N_z} q_j\hat{w}_j''''+A_0\hat{w}_1''''\right)\right]\times\right.\\
&\left.\left[\beta\sum_{j=1}^{N_x} r_j\hat{u}_j'''+\sum_{i=1}^{N_z}\sum_{j=1}^{N_z} q_iq_j\left(\hat{w}_j''\hat{w}_i''+\hat{w}_j'''\hat{w}_i'\right)+A_0\sum_{j=1}^{N_z} q_j\left(\hat{w}_j'''\hat{w}_1'+2\hat{w}_j''\hat{w}_1''+\hat{w}_j'\hat{w}_1'''\right)\right]dx\right\}\\
&-\int_0^1\left\{\hat{w}_k\left[\left(\chi_{sg}^2+\chi_{nl}^2\right)\left(\sum_{j=1}^{N_z} q_j\hat{w}_j'+A_0\hat{w}_1'\right)-3\chi_{nl}^2\chi_{sg}^2\left(\sum_{j=1}^{N_z} q_j\hat{w}_j'''+A_0\hat{w}_1'''\right)\right]\left[\beta\sum_{j=1}^{N_x} r_j\hat{u}_j''''\right.\right.\\
&\left.\left.+\sum_{i=1}^{N_z}\sum_{j=1}^{N_z} q_iq_j\left(3\hat{w}_j'''\hat{w}_i''+\hat{w}_i'\hat{w}_j''''\right)+A_0\sum_{j=1}^{N_z} q_j\left(\hat{w}_j''''\hat{w}_1'+3\hat{w}_j'''\hat{w}_1''+3\hat{w}_j''\hat{w}_1'''+\hat{w}_j'\hat{w}_1''''\right)\right]dx\right\}
\end{aligned}
$$

$$+3\chi_{nl}^2\chi_{sg}^2\int_0^1\left\{\hat{w}_k\left(\sum_{j=1}^{N_z}q_j\hat{w}_j''+A_0\hat{w}_1''\right)\left[\beta\sum_{j=1}^{N_x}r_j\hat{u}_j^{(5)}+\sum_{i=1}^{N_z}\sum_{j=1}^{N_z}q_iq_j\left(3\hat{w}_i'''\hat{w}_j'''+4\hat{w}_i''\hat{w}_j''''+\hat{w}_i'\hat{w}_j^{(5)}\right)\right.\right.$$

$$\left.\left.+A_0\sum_{j=1}^{N_z}q_j\left(\hat{w}_j^{(5)}\hat{w}_1'+4\hat{w}_j''''\hat{w}_1''+6\hat{w}_j'''\hat{w}_1'''+4\hat{w}_j''\hat{w}_1''''+\hat{w}_j'\hat{w}_1^{(5)}\right)\right]dx\right\}+$$

$$\chi_{nl}^2\chi_{sg}^2\int_0^1\left\{\hat{w}_k\left(\sum_{j=1}^{N_z}q_j\hat{w}_j'+A_0\hat{w}_1'\right)\left[\beta\sum_{j=1}^{N_x}r_j\hat{u}_j^{(6)}+\sum_{i=1}^{N_z}\sum_{j=1}^{N_z}q_iq_j\left(10\hat{w}_i'''\hat{w}_j''''+5\hat{w}_i''\hat{w}_j^{(5)}+\hat{w}_i'\hat{w}_j^{(6)}\right)\right.\right.$$

$$\left.\left.+A_0\sum_{j=1}^{N_z}q_j\left(\hat{w}_1'\hat{w}_j^{(6)}++5\hat{w}_j^{(5)}\hat{w}_1''+10\hat{w}_j''''\hat{w}_1'''+10\hat{w}_j'''\hat{w}_1''''+5\hat{w}_j''\hat{w}_1^{(5)}+\hat{w}_j'\hat{w}_1^{(6)}\right)\right]dx\right\}$$

$$-\frac{\chi_{nl}^2}{\beta}\int_0^1\hat{w}_k\left[\left(\sum_{j=1}^{N_z}q_j\hat{w}_j'+A_0\hat{w}_1'\right)\sum_{j=1}^{N_x}\ddot{r}_j\left(\chi_{nl}^2\hat{u}_j''''-\hat{u}_j''\right)+3\chi_{nl}^2\left(\sum_{j=1}^{N_z}q_j\hat{w}_j'''+A_0\hat{w}_1'''\right)\sum_{j=1}^{N_x}\ddot{r}_j\hat{u}_j''\right]dx$$

$$-\frac{\chi_{nl}^2}{\beta}\int_0^1\hat{w}_k\left(\sum_{j=1}^{N_z}q_j\hat{w}_j''+A_0\hat{w}_1''\right)\left(3\chi_{nl}^2\sum_{j=1}^{N_x}\ddot{r}_j\hat{u}_j'''-\sum_{j=1}^{N_x}\ddot{r}_j\hat{u}_j'\right)dx$$

$$-\frac{\chi_{nl}^4}{\beta}\int_0^1\left[\hat{w}_k\left(\sum_{j=1}^{N_z}q_j\hat{w}_j''''+A_0\hat{w}_1''''\right)\sum_{j=1}^{N_x}\ddot{r}_j\hat{u}_j'\right]dx=$$

$$\int_0^1\hat{w}_k\left(\sum_{j=1}^{N_z}\ddot{q}_j\hat{w}_j-\chi_{nl}^2\sum_{j=1}^{N_z}\ddot{q}_j\hat{w}_j''\right)dx-\left(\int_0^1\hat{w}_k dx\right)F_1\beta\cos(\Omega t)\quad\text{for}\quad k=1,2,\cdots N_x. \tag{19}$$

To determine the large-amplitude mechanical characteristics of geometrically imperfect nanotubes subject to a harmonic loading, a numerical scheme in the context of a continuation-based technique is employed [62, 63]. In the present nonlinear analysis, a convergence test is carried out, indicating that eight base functions for each displacement component are sufficient to meet the requirement of calculation precision. In general, a system of sixteen base functions is considered (eight base functions for *u* and eight base functions for *w*).

3. Numerical results

The influence of a geometric imperfection together with other parameters such as the nonlocal and strain gradient coefficients on the large-amplitude mechanical behaviour of nanoscale tubes is studied in this section. Let us consider an imperfect nanoscale tube of

length 100 nm. The material properties are taken as E=1.0 TPa, ν=0.19, and ρ=2300 kg/m^3. The outer and inner radii of the tube are, respectively, assumed as 0.84 and 0.5 nm. The slenderness ratio is determined as β =204.5935. In the nonlinear analysis, the modal damping ratio is chosen as ζ=0.005.

The variation of the maximum values of some transverse generalised coordinates as well as the minimum value of the second axial generalised coordinate versus the excitation-to-natural frequency ratio (excitation frequency ratio) is shown in Fig. 2. The values of the strain gradient and nonlocal coefficients are, respectively, taken as χ_{sg}=0.1 and χ_{nl} =0. The force and imperfection amplitudes are assumed as F_1=0.1 and A_0=0.8, respectively. A hardening-type nonlinearity with two saddle points (B_1 and B_2) is found for the geometrically imperfect nanoscale tube. As the excitation frequency ratio increases, the maximum value of q_1 increases until point B_1 (the first saddle point) in which the nanotube experiences a dramatic jump to a lower value of the transverse amplitude. Decreasing the excitation frequency first increases the maximum value of q_1, and then at point B_2 (the second saddle point), the nanosystem displays a sudden increase followed by a gradual reduction in q_1. In addition, from Fig. 2, modal interactions [64] around the first saddle point are clearly observed for higher generalised coordinates.

Fig. 3 illustrates the effect of χ_{sg} on the frequency-amplitude plots for imperfect nanoscale tubes. The force and imperfection amplitudes are taken as F_1=0.1 and A_0=0.8, respectively. The nonlocal effect is neglected in this figure (i.e. χ_{nl} =0). The resonant frequency of the geometrically imperfect nanotube is higher when higher values are chosen for the strain gradient coefficient. Nonetheless, the peak amplitude of the imperfect nanosystem is lower for higher values of χ_{sg}. In addition, strong modal interactions are observed, especially for

higher generalised coordinates, when the strain gradient coefficient is set to χ_{sg} =0.05. However, increasing the strain gradient effect can gradually eliminates the modal interactions.

The variation of some transverse and axial generalised coordinates of the imperfect nanoscale tube versus the excitation frequency ratio is depicted in Fig. 4; but this time, only the nonlocal effect is incorporated. The imperfection and force amplitudes are the same as those of Fig. 2. A nonlocal coefficient of 0.1 is selected for the nanotube while the strain gradient coefficient is zero. Again, a hardening-type nonlinearity with two saddle points is observed for geometrically imperfect nanotubes. However, stronger modal interactions are seen in Fig. 4 in comparison with those of Fig. 2, especially for the fifth generalised coordinate along the transverse direction. It means that the modal interaction may be overestimated when only the nonlocal effect is taken into consideration.

Figure 5 depicts the influence of χ_{nl} on the frequency-amplitude plots of imperfect nanoscale tubes. The strain gradient coefficient is set to zero. A value of 0.8 is chosen for the non-dimensional imperfection amplitude while the dimensionless force amplitude is F_1=0.1. It is found that imperfect nanotubes with higher nonlocal coefficients undergo resonance at lower excitation frequencies. Another interesting finding is that for higher nonlocal effects, the imperfect nanotube exhibits strong modal interactions (see Fig. 5c).

The variation of maximum values of some transverse generalised coordinates and the minimum value of the second axial generalised coordinate of the nanotube versus the excitation frequency ratio is demonstrated in Fig. 6; a larger imperfection amplitude (A_0=1.5) is taken into account. A value of F_1=0.14 is taken for the force amplitude. The strain gradient coefficient is taken as χ_{sg}=0.1 while the nonlocal coefficient is assumed to be zero. A

combination of softening and hardening nonlinearities with four saddle points is observed in this case. Initially, the nonlinear mechanical behaviour is of softening type which is followed by a hardening-type nonlinearity. The transverse amplitude of the imperfect nanotube increases gradually with increasing the excitation frequency ratio until point B_1 (the first saddle point) where it suddenly increases. Then, the transverse amplitude continuously increases until point B_3 (the third saddle point) in which the imperfect nanotube jumps to a lower transverse amplitude. By comparing Fig. 2 with Fig. 6, it can be concluded that a small increase in the imperfection amplitude can substantially change the nonlinear mechanical behaviour.

Figure 7 shows the influence of χ_{sg} on the large-amplitude mechanical behaviour of geometrically imperfect nanoscale tubes. The nonlocal effect is not taken into account. The imperfection amplitude and the force amplitude are set to A_0=1.5, and F_1=0.14, respectively. Imperfect nanotubes with higher strain gradient coefficients undergo resonance at higher excitation frequencies. Moreover, higher values of the strain gradient coefficient reduces the peak amplitude of both the motions along the *x* and *z* axes.

The variation of the maximum values of some transverse generalised coordinates and the minimum value of the second axial generalised coordinate versus the excitation frequency ratio is depicted in Fig. 8; only the effect of the nonlocal coefficient is taken into consideration (i.e. χ_{sg}=0.0, χ_{nl} =0.1). The imperfection and force amplitudes are the same as those mentioned above for Fig. 6. It is observed that the nonlinear behaviour is still a combination of softening and hardening types with four saddle points. Increasing the excitation frequency ratio gradually increases q_1 until point B_1 where the value of the first transverse generalised coordinate suddenly increases. Then, the value of q_1 decreases with increasing Ω/ω_1. By

comparing Fig. 6 to Fig. 8, it is seen that although the general nonlinear mechanical characteristics of the imperfect nanotube such as the number of saddle points remain the same, some details are different. Figure 9 illustrates the influence of χ_{nl} on the frequency-amplitude plots of imperfect nanoscale tubes for χ_{sg} =0.0, A_0=1.5, and f_1=0.14. It is found that in this case, non-zero nonlocal coefficients are associated with strong modal interactions, especially for higher generalised coordinates.

4. Conclusions

A nonlinear analysis has been performed in order to investigate the effect of geometrical imperfection on the large-amplitude mechanical behaviour of nanoscale tube subject to transverse distributed harmonic loading. A NSGT-based model incorporating both nonlocal and strain gradient effects was proposed to better describe the size-dependent softening and hardening behaviors of the stiffness. The EBBT as well as the Hamilton principle were utilised for deriving the coupled nonlinear equations. Galerkin's procedure as well as a continuation-based approach were lastly used to discretise the differential equations and to determine the large-amplitude mechanical characteristics, respectively.

A geometrical imperfection can significantly change the nonlinear dynamic behaviour of nanoscale tubes. When the amplitude of the geometrical imperfection is low, the nanotube displays a hardening-type nonlinearity with two saddle points. However, when a large imperfection amplitude is taken into consideration, the nanotube displays a combination of softening and hardening nonlinearities with four saddle points. Higher strain gradient coefficients are associated with higher resonant frequencies. Furthermore, it was found that increasing the strain gradient coefficient can eliminate the modal interactions. On the other

hand, higher nonlocal coefficients make the imperfect nanotube undergo resonances at lower excitation frequencies. The modal interaction is overestimated by incorporating only the nonlocal effect.

Appendix A. Verification study

To verify the present results, a linear NSGT nanotube without any geometrical imperfections is considered. For this nanotube, Eqs. (14) and (15) are reduced to only one motion equation along the transverse direction. In Fig. 10, the results are compared with those obtained by Li et al. [53] for the linear vibration of nanobeams employing the NSGT. The material and geometrical properties are given in Refs. [53, 65]. A very good agreement is observed between the reported results and the available results in the literature.

References

[1] Wang Q, Wang C. The constitutive relation and small scale parameter of nonlocal continuum mechanics for modelling carbon nanotubes. Nanotechnology. 2007;18:075702.
[2] Arash B, Wang Q. A review on the application of nonlocal elastic models in modeling of carbon nanotubes and graphenes. Computational Materials Science. 2012;51:303-13.
[3] Saadatnia Z, Esmailzadeh E. Nonlinear harmonic vibration analysis of fluid-conveying piezoelectric-layered nanotubes. Composites Part B: Engineering. 2017;123:193-209.
[4] Gul U, Aydogdu M. Noncoaxial vibration and buckling analysis of embedded double-walled carbon nanotubes by using doublet mechanics. Composites Part B: Engineering. 2018;137:60-73.
[5] Zhang Y, Liew K, Hui D. Characterizing nonlinear vibration behavior of bilayer graphene thin films. Composites Part B: Engineering. 2018;145:197-205.
[6] Barretta R, Feo L, Luciano R, de Sciarra FM, Penna R. Functionally graded Timoshenko nanobeams: a novel nonlocal gradient formulation. Composites Part B: Engineering. 2016;100:208-19.
[7] Romano G, Barretta R, Diaco M. On nonlocal integral models for elastic nano-beams. International Journal of Mechanical Sciences. 2017;131:490-9.
[8] Gholipour A, Farokhi H, Ghayesh MH. In-plane and out-of-plane nonlinear size-dependent dynamics of microplates. Nonlinear Dynamics. 2015;79:1771-85.
[9] Ghayesh MH, Amabili M, Farokhi H. Three-dimensional nonlinear size-dependent behaviour of Timoshenko microbeams. International Journal of Engineering Science. 2013;71:1-14.
[10] Ghayesh MH, Farokhi H. Nonlinear dynamics of microplates. International Journal of Engineering Science. 2015;86:60-73.
[11] Reddy J. Nonlocal theories for bending, buckling and vibration of beams. International Journal of Engineering Science. 2007;45:288-307.

[12] Preethi K, Rajagopal A, Reddy JN. Surface and non-local effects for non-linear analysis of Timoshenko beams. International Journal of Non-Linear Mechanics. 2015;76:100-11.
[13] Farajpour A, Rastgoo A, Mohammadi M. Vibration, buckling and smart control of microtubules using piezoelectric nanoshells under electric voltage in thermal environment. Physica B: Condensed Matter. 2017;509:100-14.
[14] Farajpour MR, Shahidi A, Farajpour A. Resonant frequency tuning of nanobeams by piezoelectric nanowires under thermo-electro-magnetic field: A theoretical study. Micro & Nano Letters. 2018.
[15] Guo S, He Y, Liu D, Lei J, Shen L, Li Z. Torsional vibration of carbon nanotube with axial velocity and velocity gradient effect. International Journal of Mechanical Sciences. 2016;119:88-96.
[16] Eptaimeros K, Koutsoumaris CC, Tsamasphyros G. Nonlocal integral approach to the dynamical response of nanobeams. International Journal of Mechanical Sciences. 2016;115:68-80.
[17] Guo S, He Y, Liu D, Lei J, Li Z. Dynamic transverse vibration characteristics and vibro-buckling analyses of axially moving and rotating nanobeams based on nonlocal strain gradient theory. Microsystem Technologies. 2018;24:963-77.
[18] Li L, Tang H, Hu Y. The effect of thickness on the mechanics of nanobeams. International Journal of Engineering Science. 2018;123:81-91.
[19] Ma L, Ke L, Reddy J, Yang J, Kitipornchai S, Wang Y. Wave propagation characteristics in magneto-electro-elastic nanoshells using nonlocal strain gradient theory. Composite Structures. 2018;199:10-23.
[20] Lei J, He Y, Guo S, Li Z, Liu D. Size-dependent vibration of nickel cantilever microbeams: experiment and gradient elasticity. AIP Advances. 2016;6:105202.
[21] Li Z, He Y, Lei J, Guo S, Liu D, Wang L. A standard experimental method for determining the material length scale based on modified couple stress theory. International Journal of Mechanical Sciences. 2018;141:198-205.
[22] Farshidianfar A, Soltani P. Nonlinear flow-induced vibration of a SWCNT with a geometrical imperfection. Computational Materials Science. 2012;53:105-16.
[23] Wang B, Deng Z-c, Zhang K. Nonlinear vibration of embedded single-walled carbon nanotube with geometrical imperfection under harmonic load based on nonlocal Timoshenko beam theory. Applied Mathematics and Mechanics. 2013;34:269-80.
[24] Mohammadi H, Mahzoon M, Mohammadi M, Mohammadi M. Postbuckling instability of nonlinear nanobeam with geometric imperfection embedded in elastic foundation. Nonlinear Dynamics. 2014;76:2005-16.
[25] Barati MR, Zenkour AM. Investigating post-buckling of geometrically imperfect metal foam nanobeams with symmetric and asymmetric porosity distributions. Composite Structures. 2017;182:91-8.
[26] Jalali S, Jomehzadeh E, Pugno N. Influence of out-of-plane defects on vibration analysis of graphene: Molecular Dynamics and Non-local Elasticity approaches. Superlattices and Microstructures. 2016;91:331-44.
[27] Rafiee M, He X, Liew K. Non-linear dynamic stability of piezoelectric functionally graded carbon nanotube-reinforced composite plates with initial geometric imperfection. International Journal of Non-Linear Mechanics. 2014;59:37-51.
[28] Arefi A, Salimi M. Investigations on vibration and buckling of carbon nanotubes with small initial curvature by nonlocal elasticity theory. Fullerenes, Nanotubes and Carbon Nanostructures. 2015;23:105-12.
[29] Wang C, Lan L, Liu Y, Tan H, He X. Vibration characteristics of wrinkled single-layered graphene sheets. International Journal of Solids and Structures. 2013;50:1812-23.
[30] Sahmani S, Fattahi A. Imperfection sensitivity of the size-dependent nonlinear instability of axially loaded FGM nanopanels in thermal environments. Acta Mechanica. 2017;228:3789-810.
[31] Farokhi H, Ghayesh MH, Amabili M. Nonlinear dynamics of a geometrically imperfect microbeam based on the modified couple stress theory. International Journal of Engineering Science. 2013;68:11-23.

[32] Farokhi H, Ghayesh MH. Thermo-mechanical dynamics of perfect and imperfect Timoshenko microbeams. International Journal of Engineering Science. 2015;91:12-33.
[33] Farokhi H, Ghayesh MH. Nonlinear dynamical behaviour of geometrically imperfect microplates based on modified couple stress theory. International Journal of Mechanical Sciences. 2015;90:133-44.
[34] Zhu X, Li L. Closed form solution for a nonlocal strain gradient rod in tension. International Journal of Engineering Science. 2017;119:16-28.
[35] Li L, Hu Y, Ling L. Wave propagation in viscoelastic single-walled carbon nanotubes with surface effect under magnetic field based on nonlocal strain gradient theory. Physica E: Low-dimensional Systems and Nanostructures. 2016;75:118-24.
[36] Wang J, Shen H, Zhang B, Liu J, Zhang Y. Complex modal analysis of transverse free vibrations for axially moving nanobeams based on the nonlocal strain gradient theory. Physica E: Low-dimensional Systems and Nanostructures. 2018;101:85-93.
[37] Wang J, Shen H, Zhang B, Liu J. Studies on the dynamic stability of an axially moving nanobeam based on the nonlocal strain gradient theory. Modern Physics Letters B. 2018:1850167.
[38] Şimşek M. Nonlinear free vibration of a functionally graded nanobeam using nonlocal strain gradient theory and a novel Hamiltonian approach. International Journal of Engineering Science. 2016;105:12-27.
[39] Sahmani S, Aghdam M. Nonlocal strain gradient shell model for axial buckling and postbuckling analysis of magneto-electro-elastic composite nanoshells. Composites Part B: Engineering. 2018;132:258-74.
[40] Farajpour A, Rastgoo A. Influence of carbon nanotubes on the buckling of microtubule bundles in viscoelastic cytoplasm using nonlocal strain gradient theory. Results in physics. 2017;7:1367-75.
[41] Ebrahimi F, Barati MR. Vibration analysis of nonlocal strain gradient embedded single-layer graphene sheets under nonuniform in-plane loads. Journal of Vibration and Control. 2017:1077546317734083.
[42] Eringen AC. Nonlocal continuum field theories: Springer Science & Business Media, 2002.
[43] Farajpour M, Shahidi A, Farajpour A. A nonlocal continuum model for the biaxial buckling analysis of composite nanoplates with shape memory alloy nanowires. Materials Research Express. 2018;5:035026.
[44] Farajpour M, Shahidi A, Hadi A, Farajpour A. Influence of initial edge displacement on the nonlinear vibration, electrical and magnetic instabilities of magneto-electro-elastic nanofilms. Mechanics of Advanced Materials and Structures. 2018:1-13.
[45] Farajpour A, Rastgoo A, Farajpour M. Nonlinear buckling analysis of magneto-electro-elastic CNT-MT hybrid nanoshells based on the nonlocal continuum mechanics. Composite Structures. 2017;180:179-91.
[46] Reddy J. Nonlocal nonlinear formulations for bending of classical and shear deformation theories of beams and plates. International Journal of Engineering Science. 2010;48:1507-18.
[47] Ghayesh MH, Amabili M, Farokhi H. Nonlinear forced vibrations of a microbeam based on the strain gradient elasticity theory. International Journal of Engineering Science. 2013;63:52-60.
[48] Ghayesh MH, Farokhi H, Amabili M. Nonlinear dynamics of a microscale beam based on the modified couple stress theory. Composites Part B: Engineering. 2013;50:318-24.
[49] Ghayesh MH, Farokhi H. Chaotic motion of a parametrically excited microbeam. International Journal of Engineering Science. 2015;96:34-45.
[50] Farajpour M, Shahidi A, Tabataba'i-Nasab F, Farajpour A. Vibration of initially stressed carbon nanotubes under magneto-thermal environment for nanoparticle delivery via higher-order nonlocal strain gradient theory. The European Physical Journal Plus. 2018;133:219.
[51] Farajpour MR, Rastgoo A, Farajpour A, Mohammadi M. Vibration of piezoelectric nanofilm-based electromechanical sensors via higher-order non-local strain gradient theory. Micro & Nano Letters. 2016;11:302-7.

[52] Lim C, Zhang G, Reddy J. A higher-order nonlocal elasticity and strain gradient theory and its applications in wave propagation. Journal of the Mechanics and Physics of Solids. 2015;78:298-313.
[53] Li X, Li L, Hu Y, Ding Z, Deng W. Bending, buckling and vibration of axially functionally graded beams based on nonlocal strain gradient theory. Composite Structures. 2017;165:250-65.
[54] Zhang L, Zhang Y, Liew K. Vibration analysis of quadrilateral graphene sheets subjected to an in-plane magnetic field based on nonlocal elasticity theory. Composites Part B: Engineering. 2017;118:96-103.
[55] Mercan K, Civalek Ö. Buckling analysis of Silicon carbide nanotubes (SiCNTs) with surface effect and nonlocal elasticity using the method of HDQ. Composites Part B: Engineering. 2017;114:34-45.
[56] Mehralian F, Beni YT, Zeverdejani MK. Nonlocal strain gradient theory calibration using molecular dynamics simulation based on small scale vibration of nanotubes. Physica B: Condensed Matter. 2017;514:61-9.
[57] Mehralian F, Beni YT, Zeverdejani MK. Calibration of nonlocal strain gradient shell model for buckling analysis of nanotubes using molecular dynamics simulations. Physica B: Condensed Matter. 2017;521:102-11.
[58] Ghayesh MH, Farokhi H, Amabili M. Nonlinear behaviour of electrically actuated MEMS resonators. International Journal of Engineering Science. 2013;71:137-55.
[59] Ghayesh MH, Farokhi H, Alici G. Size-dependent performance of microgyroscopes. International Journal of Engineering Science. 2016;100:99-111.
[60] Malekzadeh P, Farajpour A. Axisymmetric free and forced vibrations of initially stressed circular nanoplates embedded in an elastic medium. Acta Mechanica. 2012;223:2311-30.
[61] Ghayesh MH, Farokhi H, Farajpour A. Chaotic oscillations of viscoelastic microtubes conveying pulsatile fluid. Microfluidics and Nanofluidics. 2018;22:72.
[62] Allgower EL, Georg K. Introduction to numerical continuation methods: SIAM, 2003.
[63] Mittelmann H, Roose D. Continuation techniques and bifurcation problems. 1989.
[64] Ghayesh MH, Farokhi H, Amabili M. In-plane and out-of-plane motion characteristics of microbeams with modal interactions. Composites Part B: Engineering. 2014;60:423-39.
[65] Li L, Li X, Hu Y. Free vibration analysis of nonlocal strain gradient beams made of functionally graded material. International Journal of Engineering Science. 2016;102:77-92.

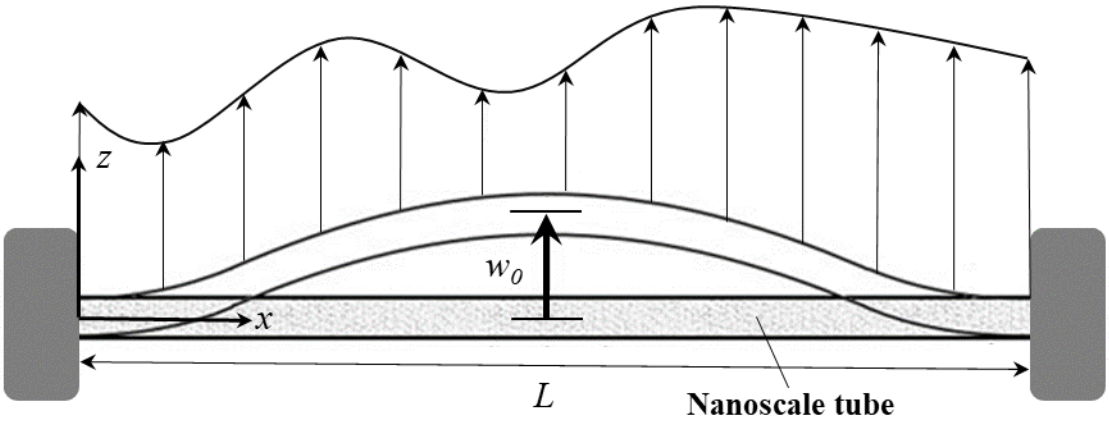

Fig. 1. Schematic representation of a geometrically imperfect nanoscale tube subject to a harmonic loading.

(a)

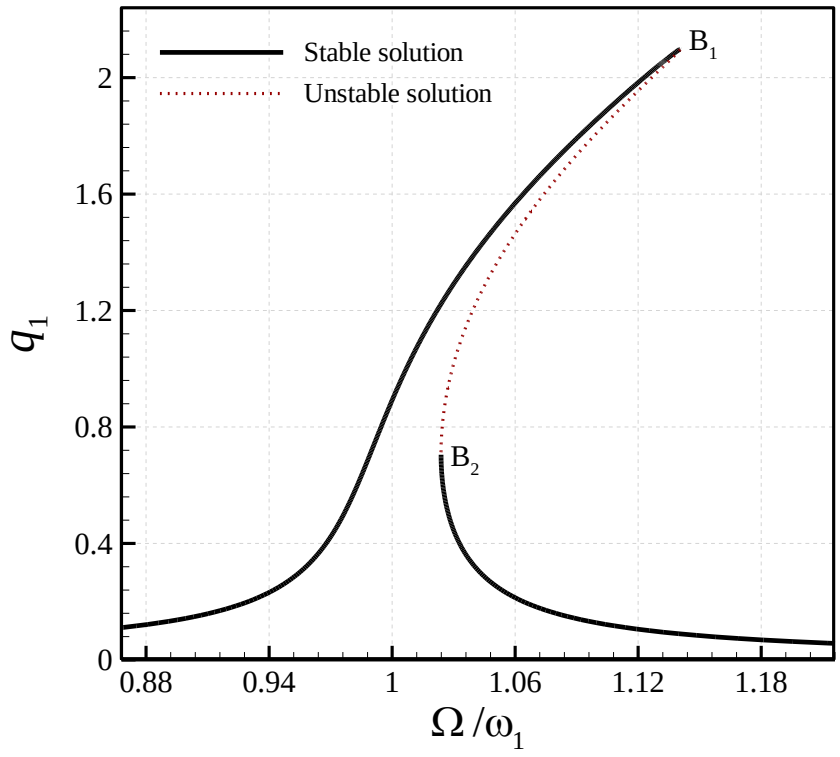
Stable solution
Unstable solution
B1
B2
q1
Ω /ω1
0
0.4
0.8
1.2
1.6
2
0.88
0.94
1
1.06
1.12
1.18

(b)

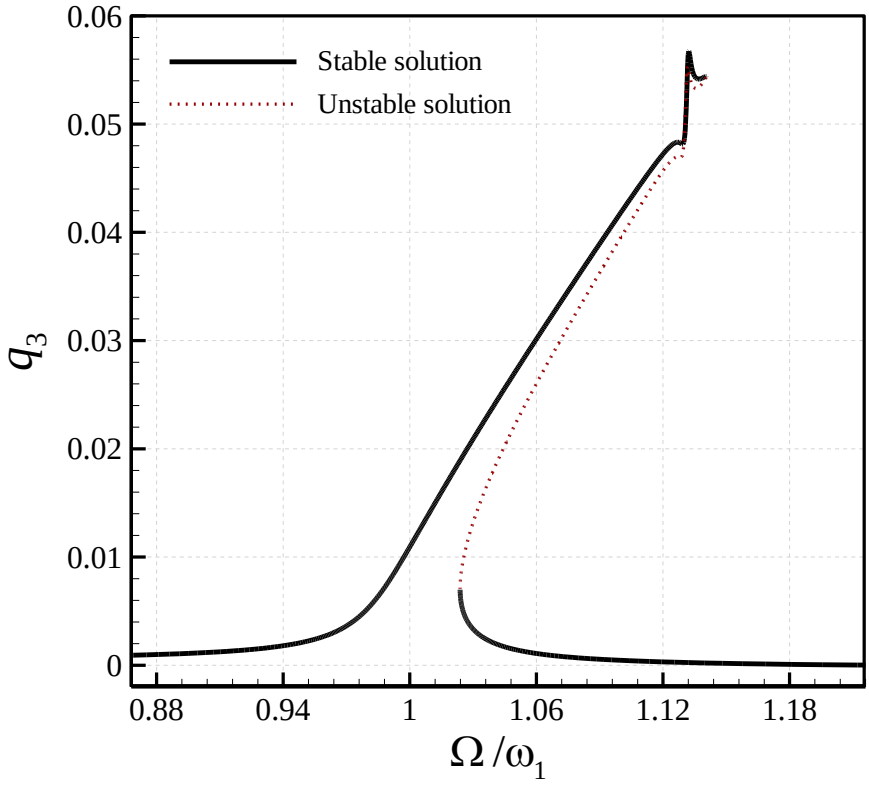
Stable solution
Unstable solution
q3
Ω /ω1
0
0.01
0.02
0.03
0.04
0.05
0.06
0.88
0.94
1
1.06
1.12
1.18

(c)

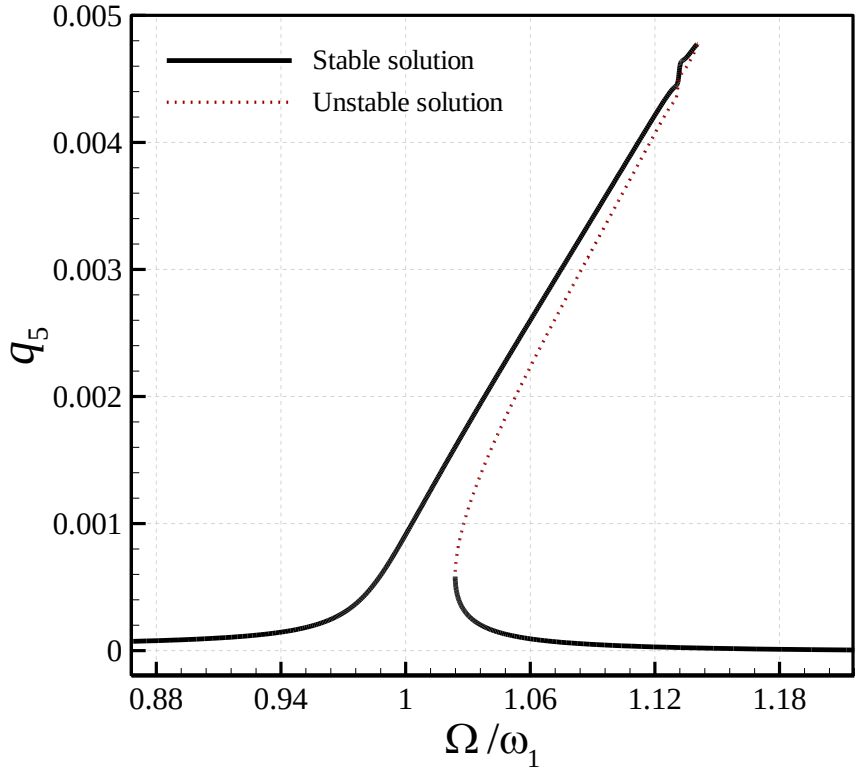

(d)

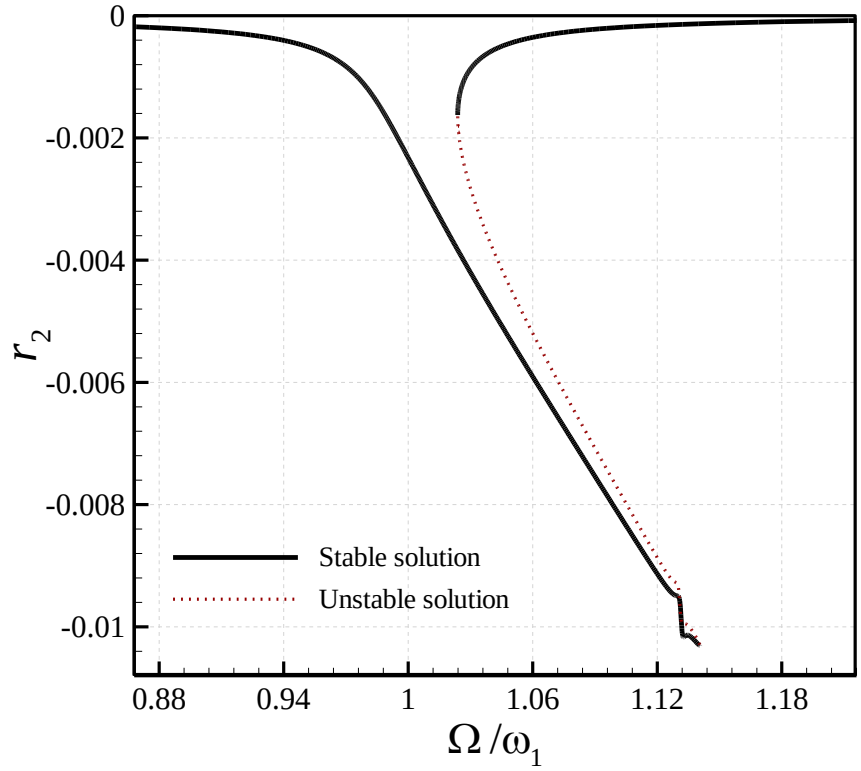

Fig. 2. Frequency-amplitude plots of the geometrically imperfect nanotube; (a-c) the maximum of q_1, q_2, and q_3, respectively; (d) the minimum of r_2; for non-zero χ_{sg} and A_0=0.8.

(a)

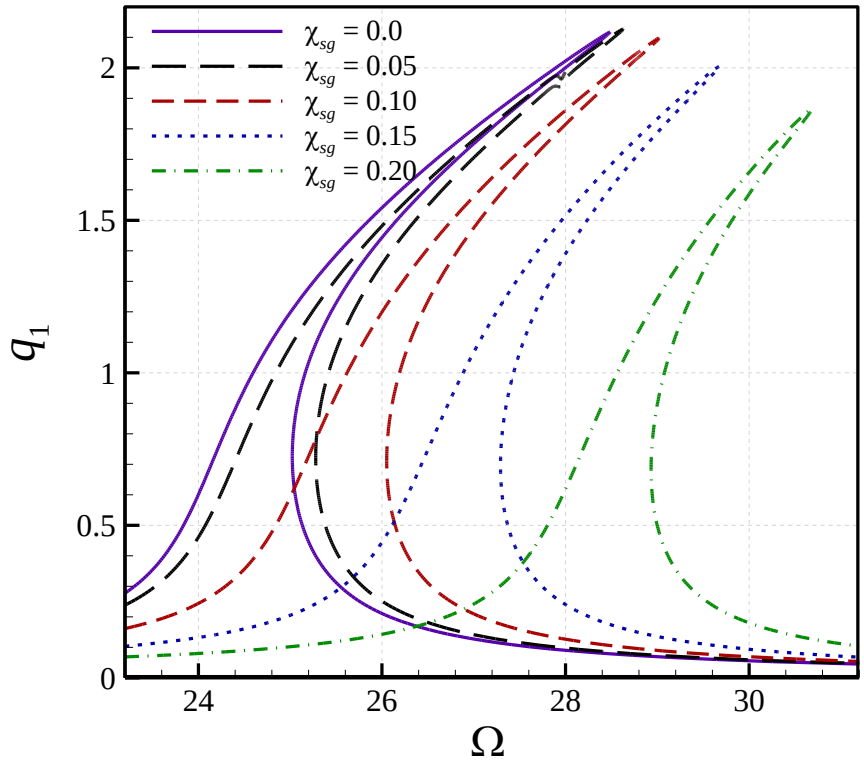
χ_{sg} = 0.0
χ_{sg} = 0.05
χ_{sg} = 0.10
χ_{sg} = 0.15
χ_{sg} = 0.20
q_1
Ω
0
0.5
1
1.5
2
24
26
28
30

(b)

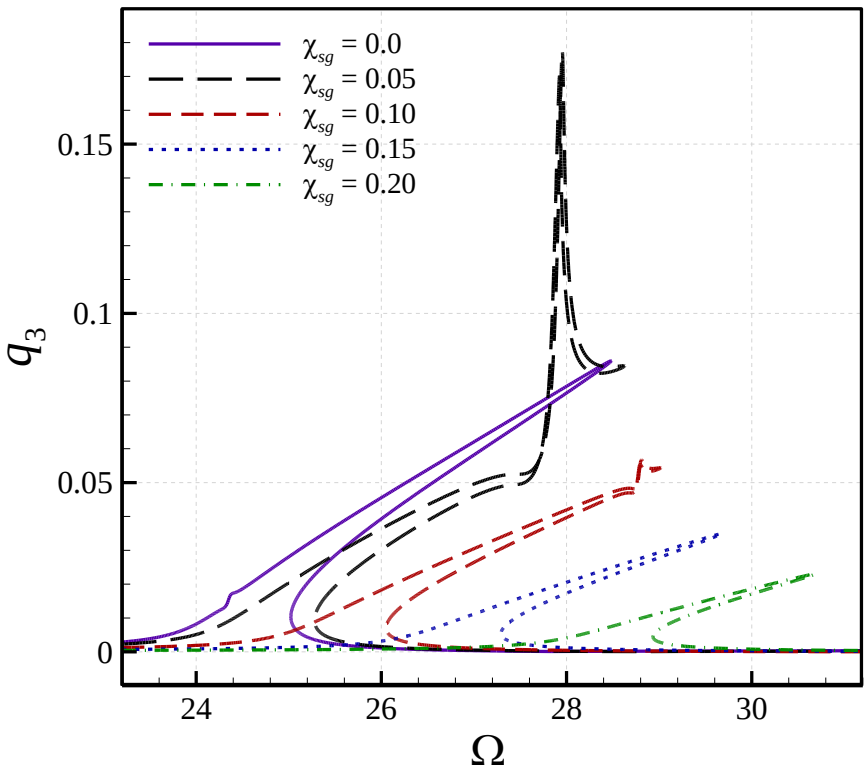
χ_{sg} = 0.0
χ_{sg} = 0.05
χ_{sg} = 0.10
χ_{sg} = 0.15
χ_{sg} = 0.20
q_3
Ω
0
0.05
0.1
0.15
24
26
28
30

(c)

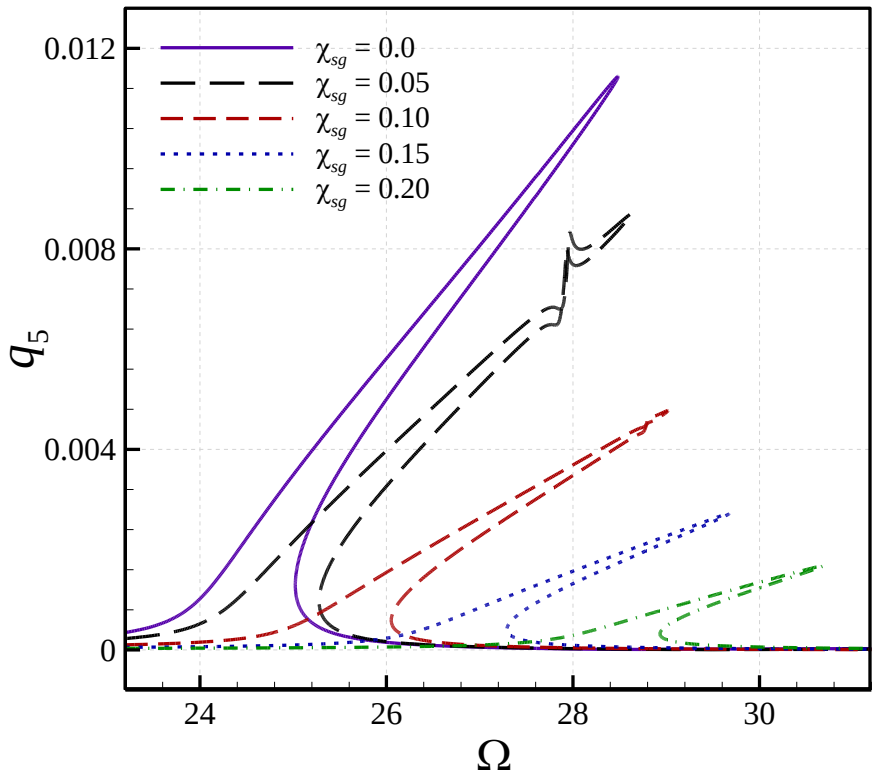

(d)

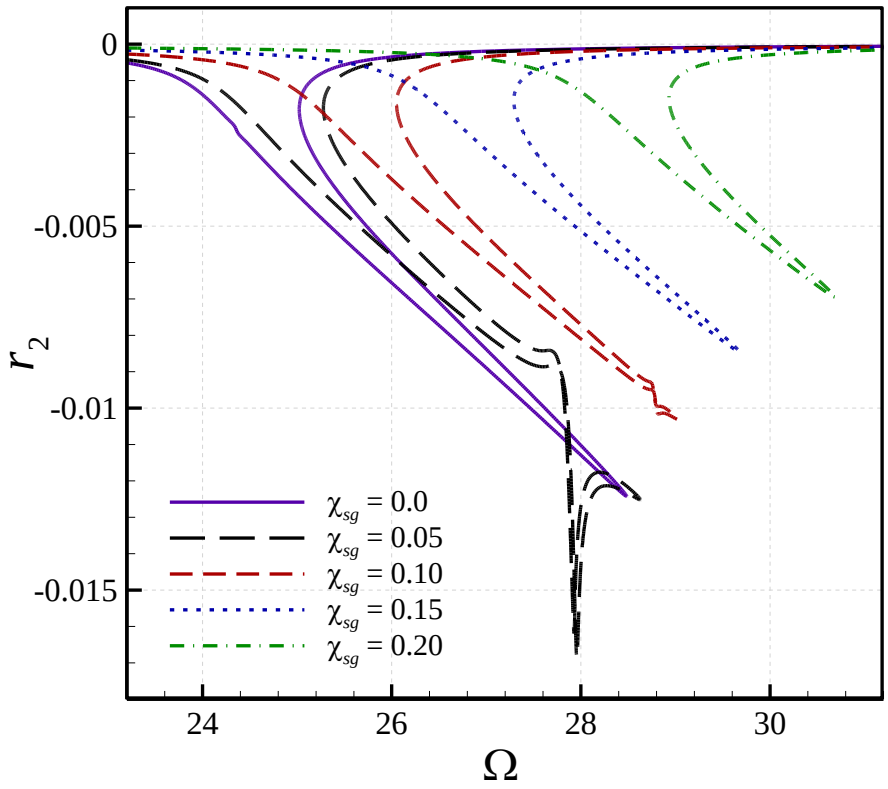

Fig. 3. Strain gradient effects on frequency-amplitude plots of the geometrically imperfect nanotube; (a-c) the maximum of q_1, q_2, and q_3, respectively; (d) the minimum of r_2 for A_0=0.8.

(a)

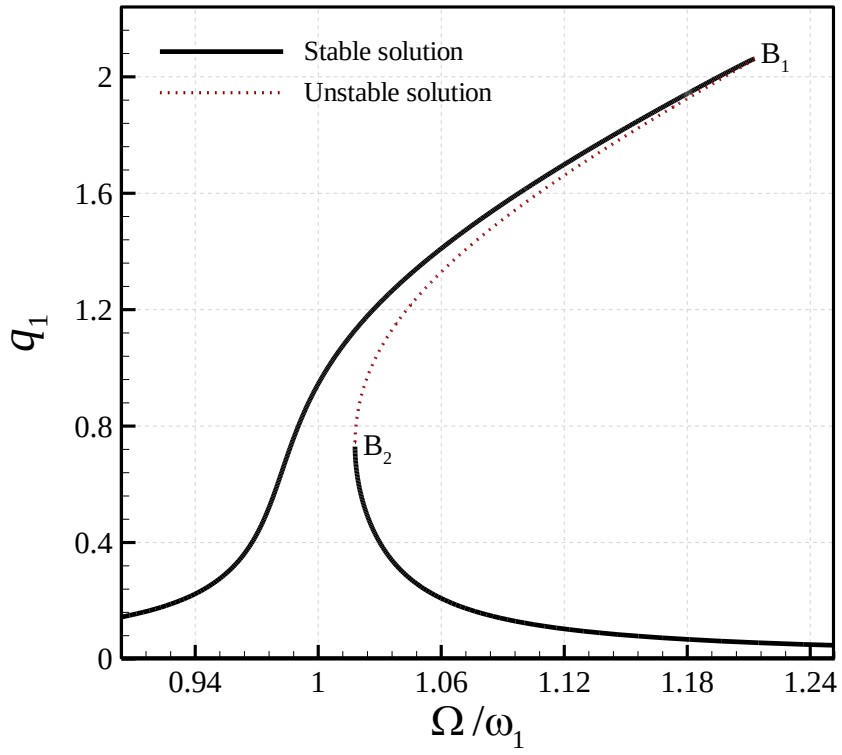
Stable solution
Unstable solution
B1
B2
q1
Ω /ω1
0
0.4
0.8
1.2
1.6
2
0.94
1
1.06
1.12
1.18
1.24

(b)

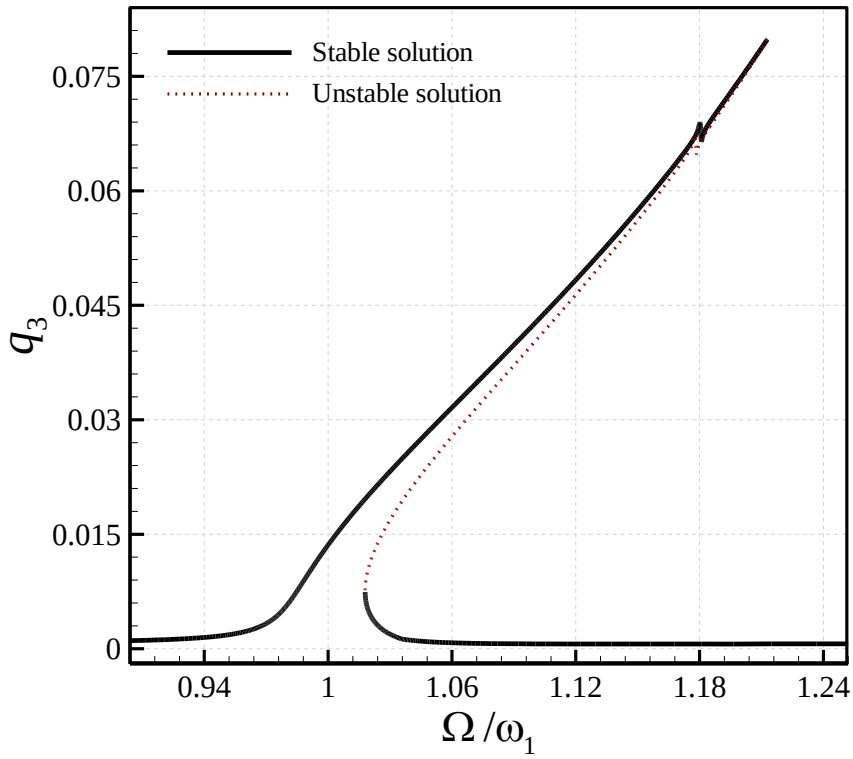
Stable solution
Unstable solution
q3
Ω /ω1
0
0.015
0.03
0.045
0.06
0.075
0.94
1
1.06
1.12
1.18
1.24

(c)

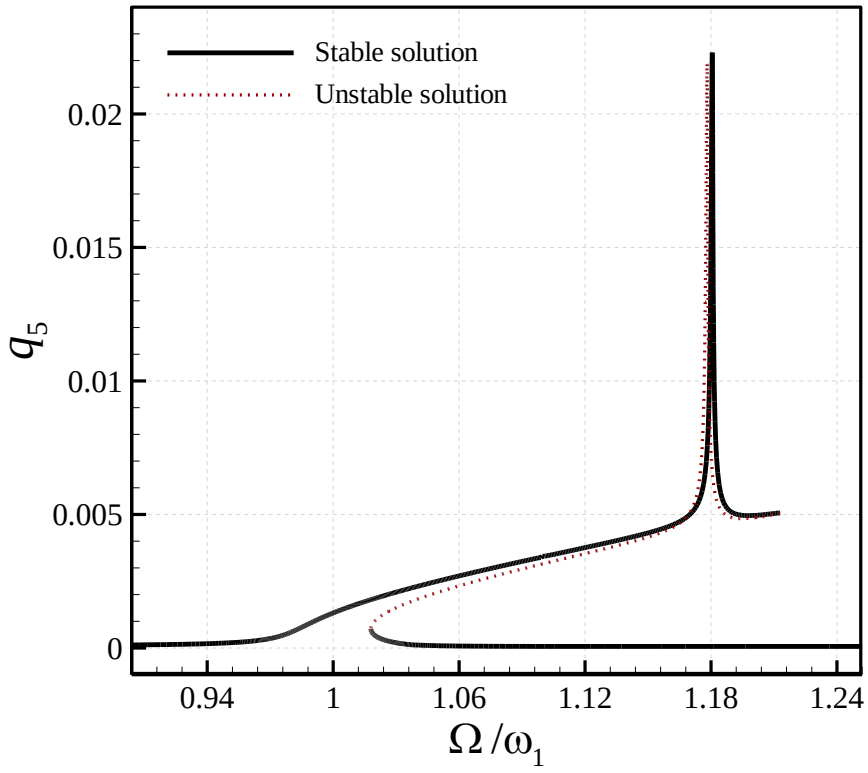

(d)

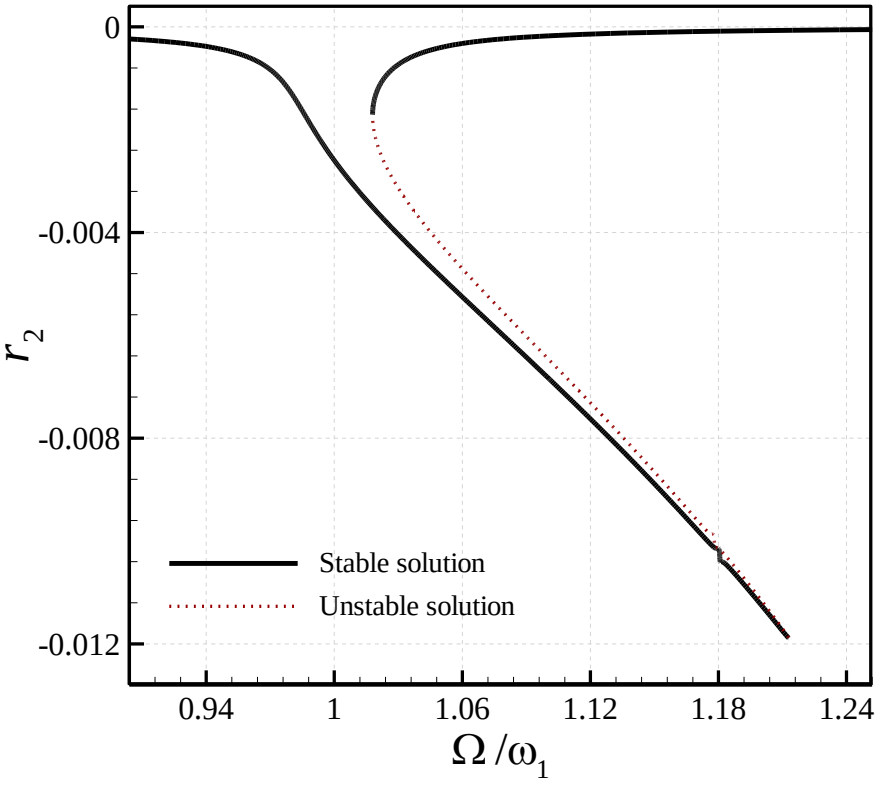

Fig. 4. Frequency-amplitude plots of the geometrically imperfect nanotube; (a-c) the maximum of q_1, q_2, and q_3, respectively; (d) the minimum of r_2 for non-zero χ_{nl} and A_0=0.8.

(a)

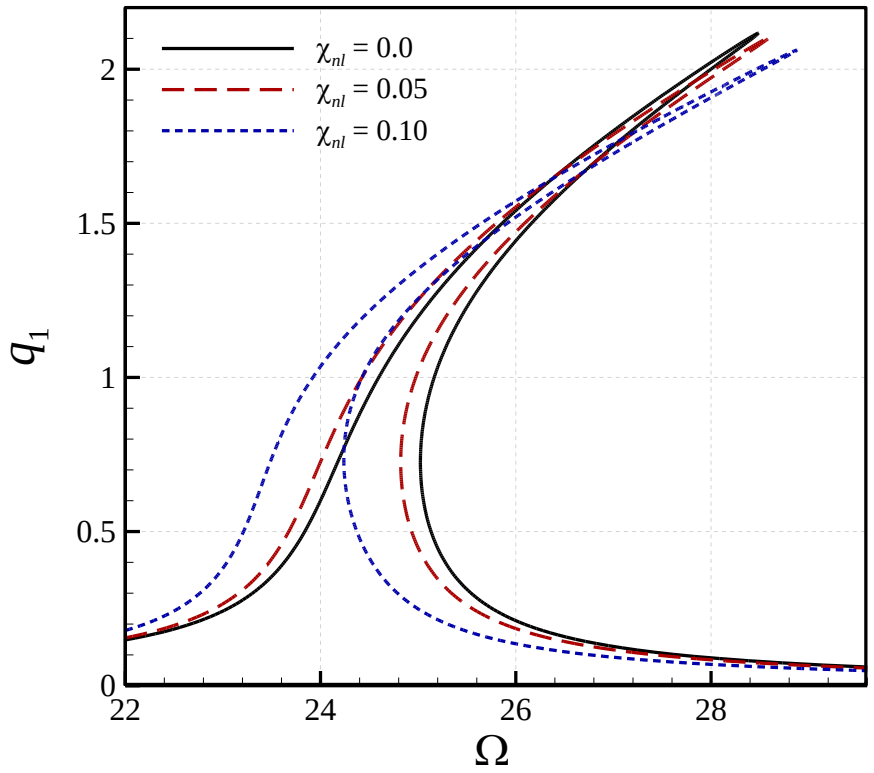
χ_{nl} = 0.0
χ_{nl} = 0.05
χ_{nl} = 0.10
q_1
Ω
0
0.5
1
1.5
2
22
24
26
28

(b)

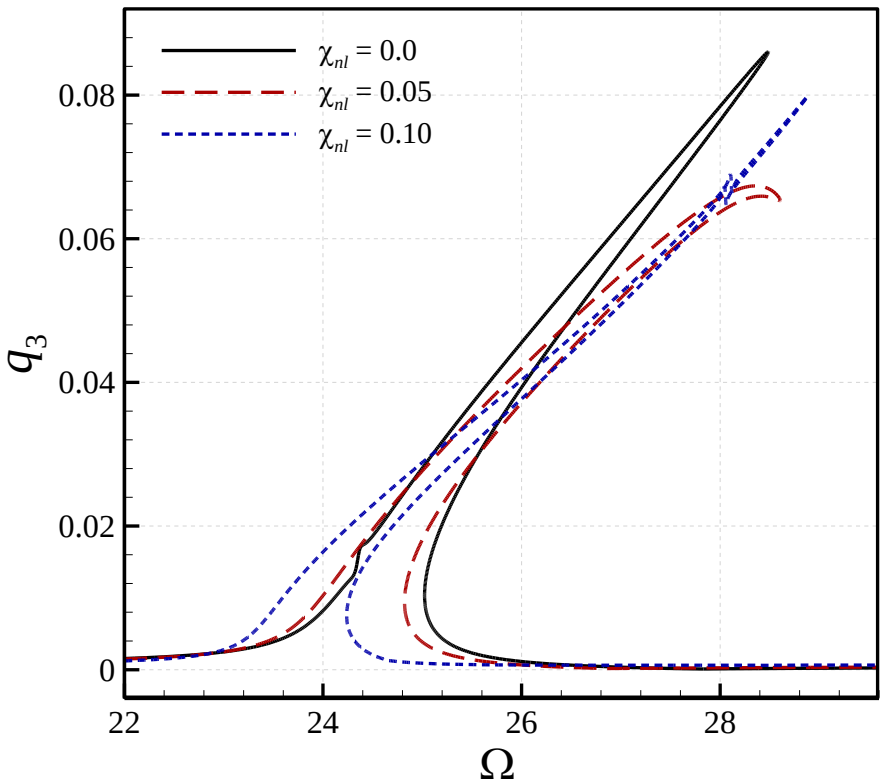
χ_{nl} = 0.0
χ_{nl} = 0.05
χ_{nl} = 0.10
q_3
Ω
0
0.02
0.04
0.06
0.08
22
24
26
28

(c)

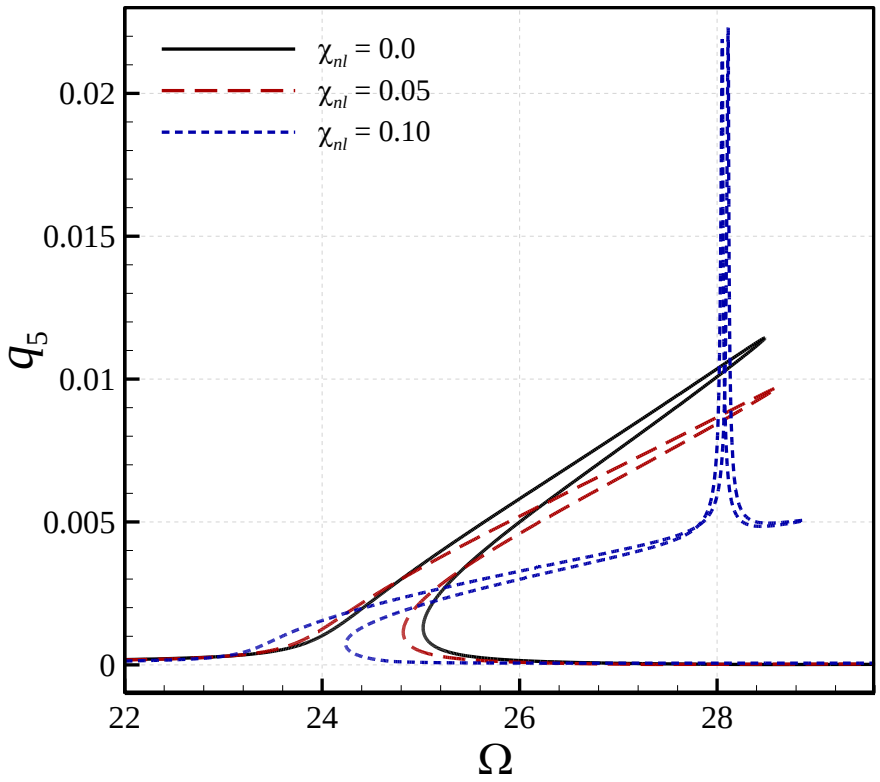

(d)

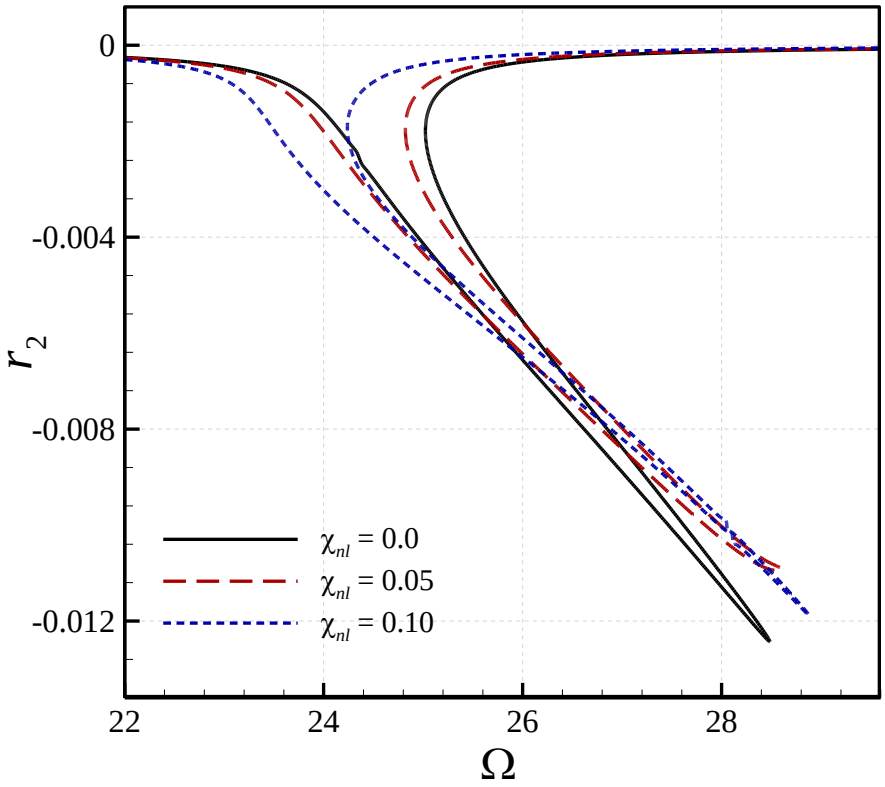

Fig. 5. Nonlocal effects on frequency-amplitude plots of the geometrically imperfect nanotube; (a-c) the maximum of q_1, q_2, and q_3, respectively; (d) the minimum of r_2 for A_0=0.8.

(a)

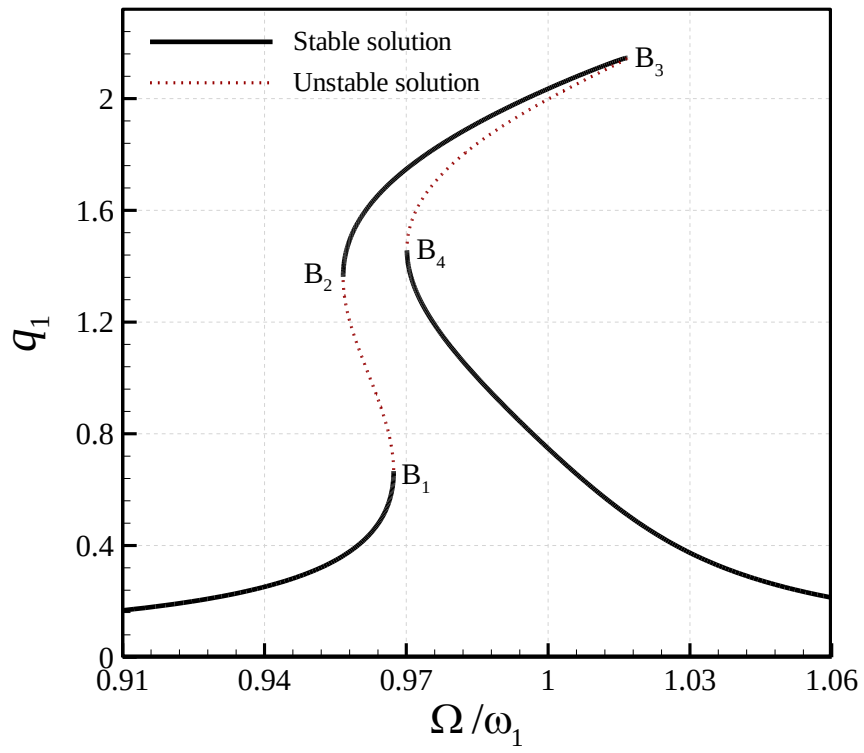
Stable solution
Unstable solution
B3
B4
B2
B1
q1
Ω /ω1
0
0.4
0.8
1.2
1.6
2
0.91
0.94
0.97
1
1.03
1.06

(b)

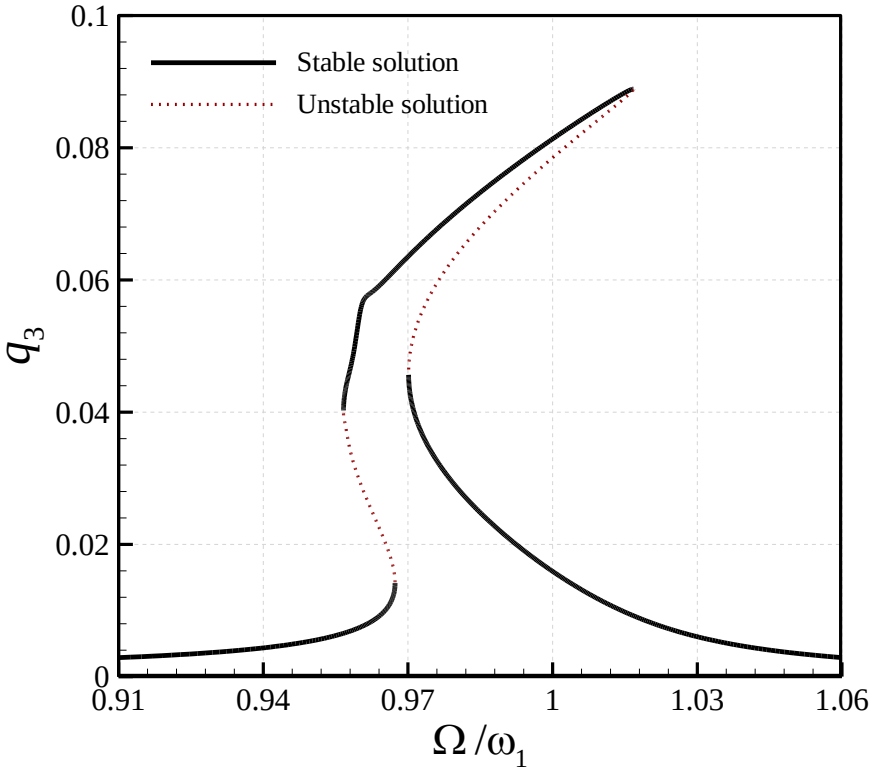
Stable solution
Unstable solution
q3
Ω /ω1
0
0.02
0.04
0.06
0.08
0.1
0.91
0.94
0.97
1
1.03
1.06

(c)

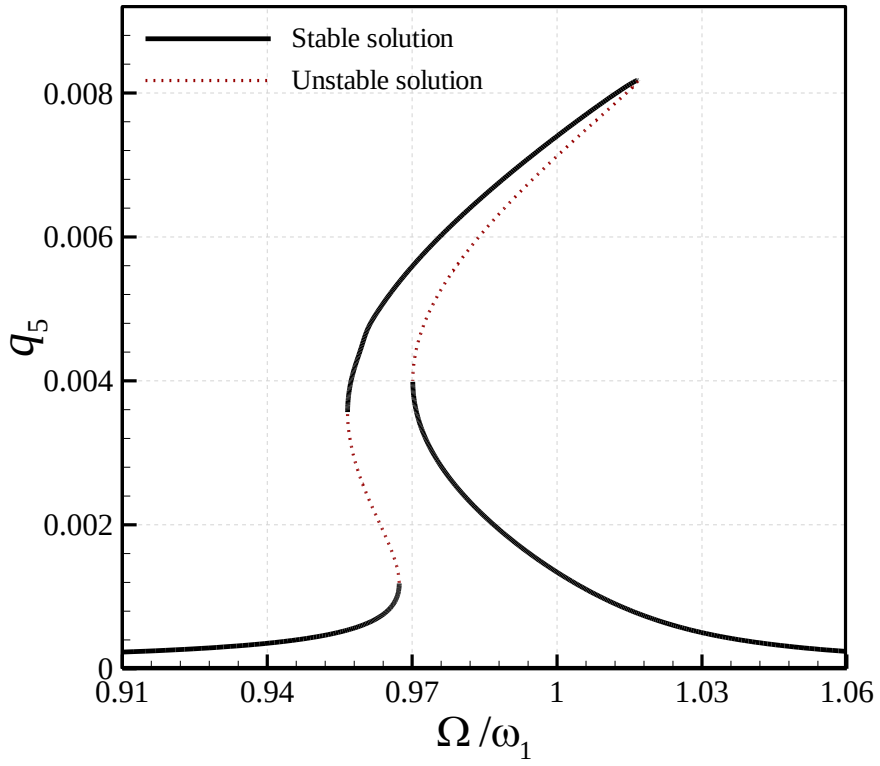

(d)

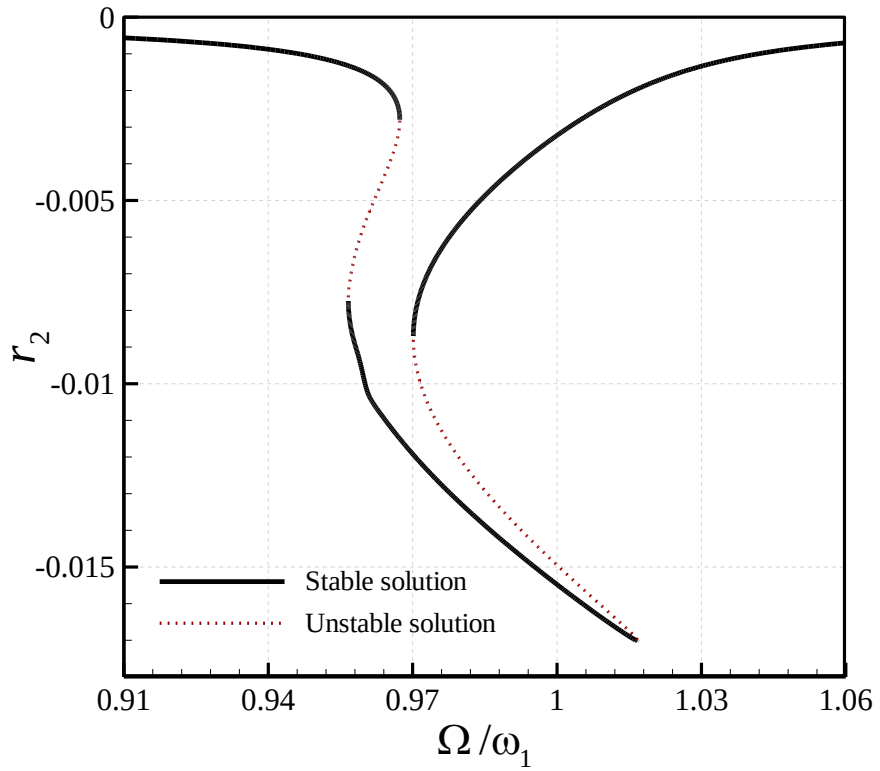

Fig. 6. Frequency-amplitude plots of the geometrically imperfect nanotube; (a-c) the maximum of q_1, q_2, and q_3, respectively; (d) the minimum of r_2 for non-zero χ_{sg} and A_0=1.5.

(a)

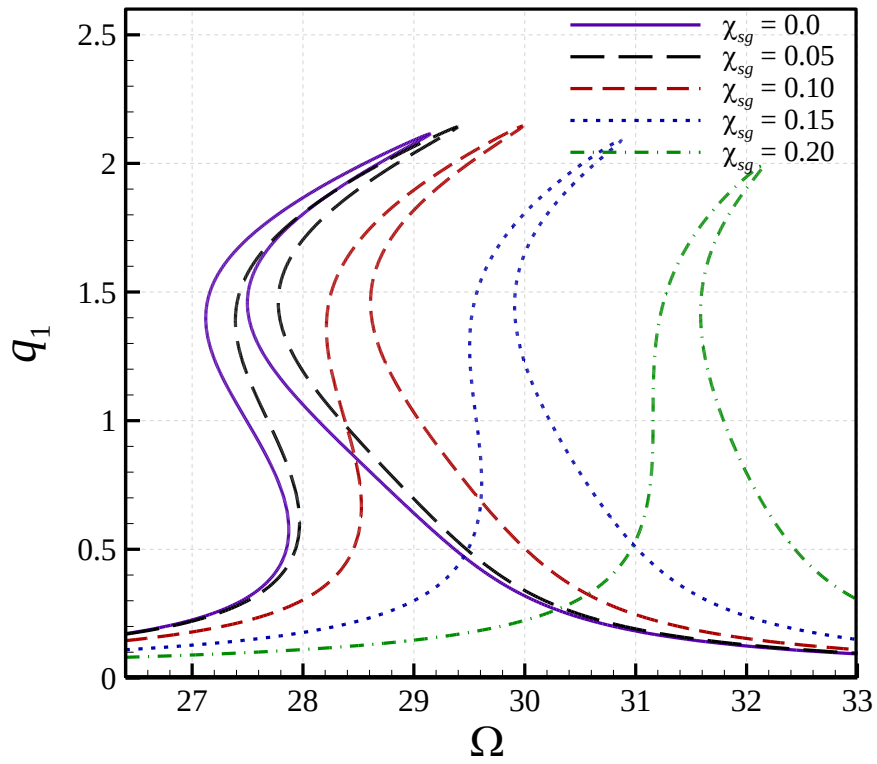
2.5
2
1.5
1
0.5
0
q_1
27
28
29
30
31
32
33
Ω
χ_{sg} = 0.0
χ_{sg} = 0.05
χ_{sg} = 0.10
χ_{sg} = 0.15
χ_{sg} = 0.20

(b)

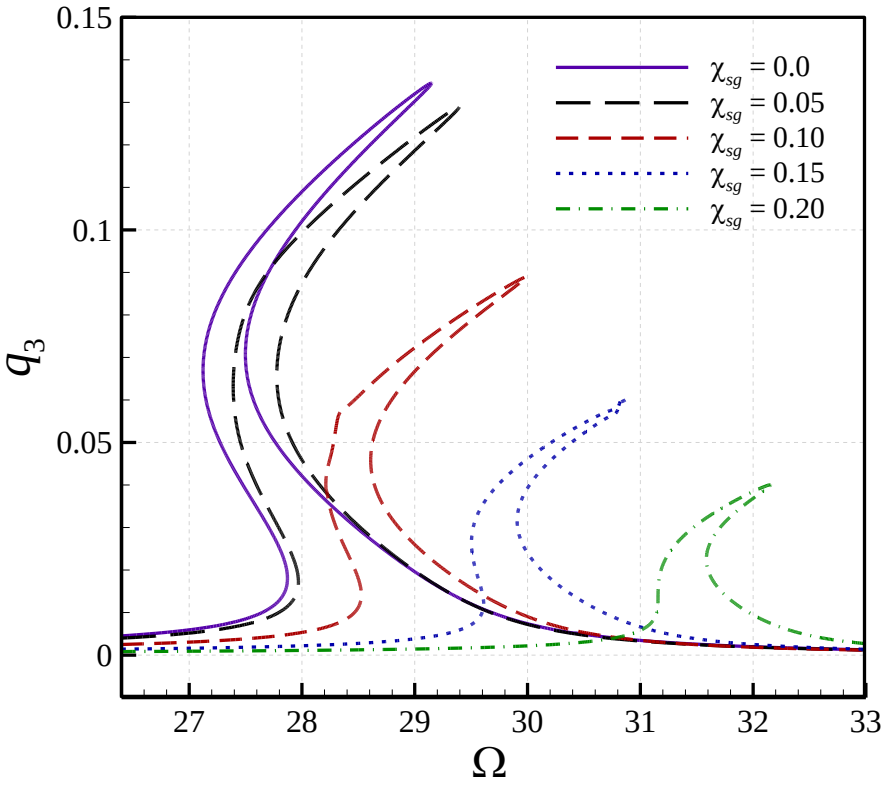
0.15
0.1
0.05
0
q_3
27
28
29
30
31
32
33
Ω
χ_{sg} = 0.0
χ_{sg} = 0.05
χ_{sg} = 0.10
χ_{sg} = 0.15
χ_{sg} = 0.20

(c)

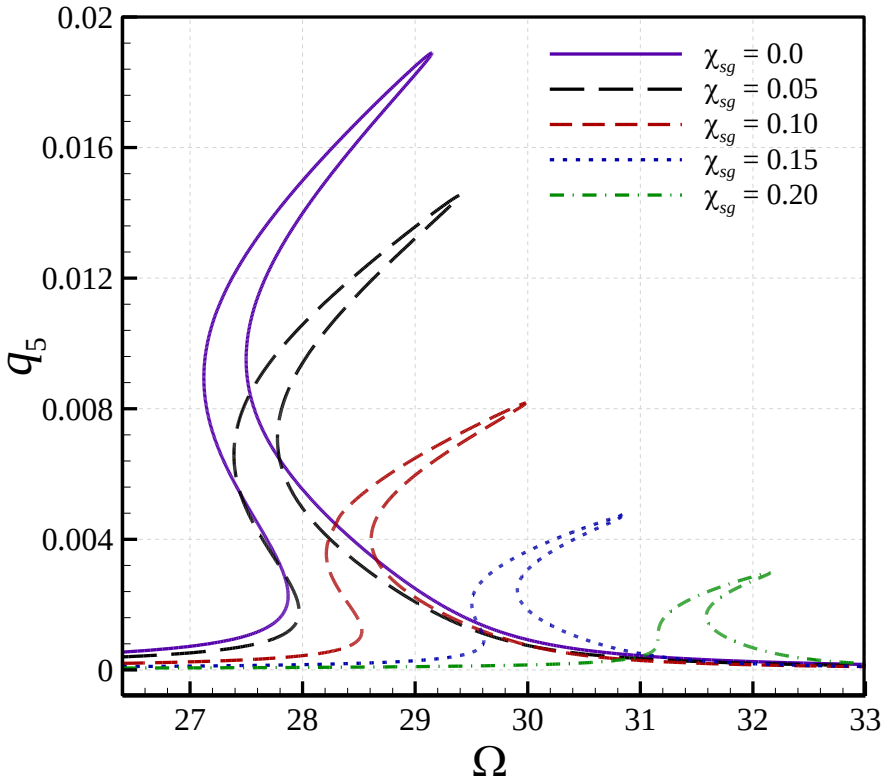

(d)

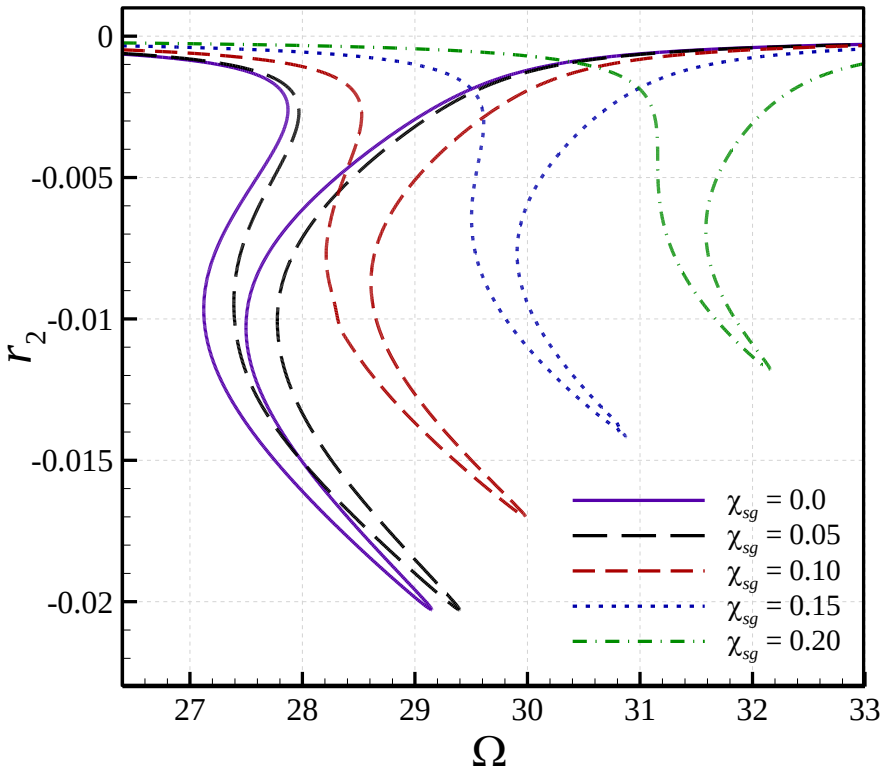

Fig. 7. Strain gradient effects on frequency-amplitude plots of the geometrically imperfect nanotube; (a-c) the maximum of q_1, q_2, and q_3, respectively; (d) the minimum of r_2 for A_0=1.5.

(a)

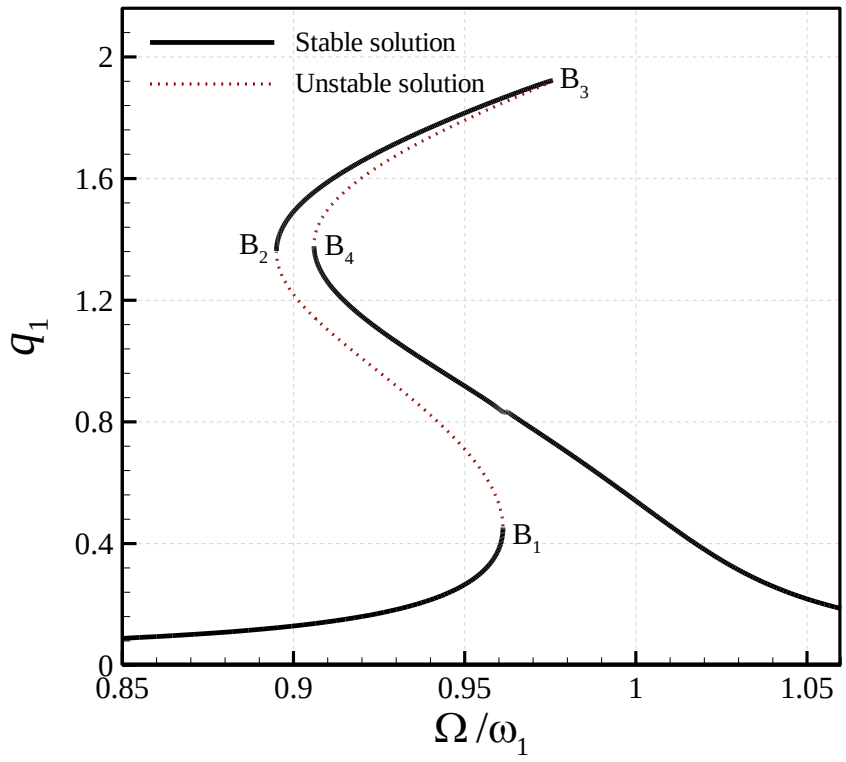
Stable solution
Unstable solution
B3
B2
B4
B1
q1
Ω /ω1
0
0.4
0.8
1.2
1.6
2
0.85
0.9
0.95
1
1.05

(b)

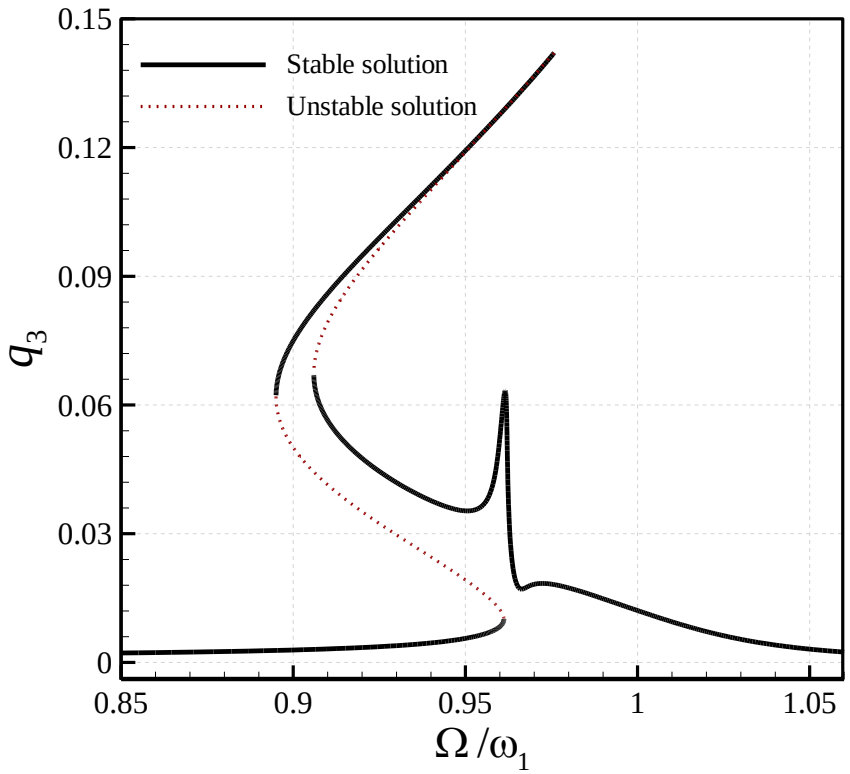
Stable solution
Unstable solution
q3
Ω /ω1
0
0.03
0.06
0.09
0.12
0.15
0.85
0.9
0.95
1
1.05

(c)

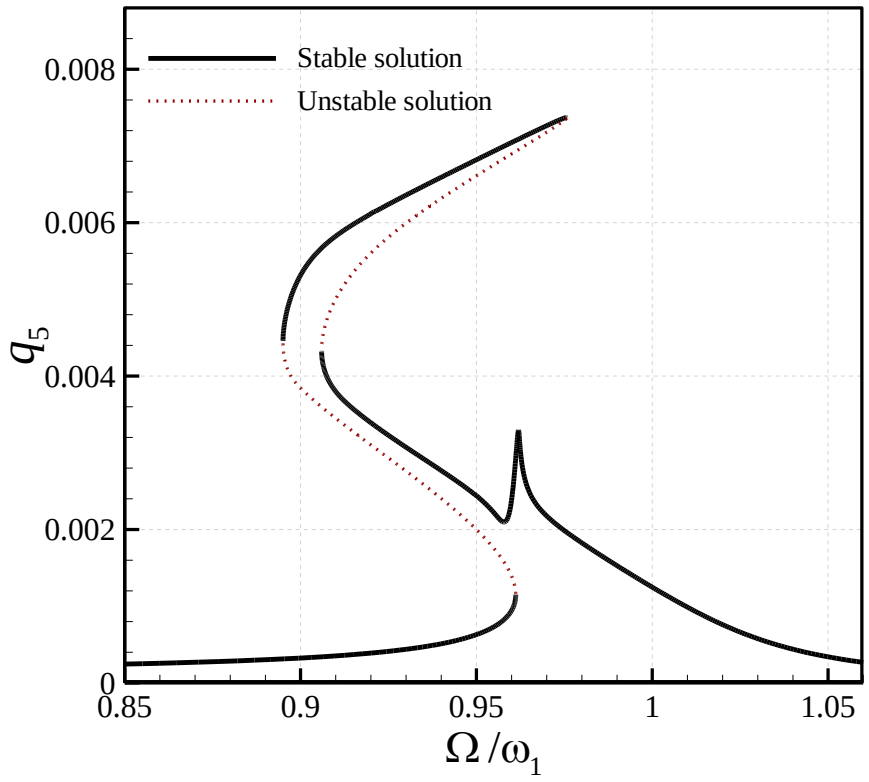

(d)

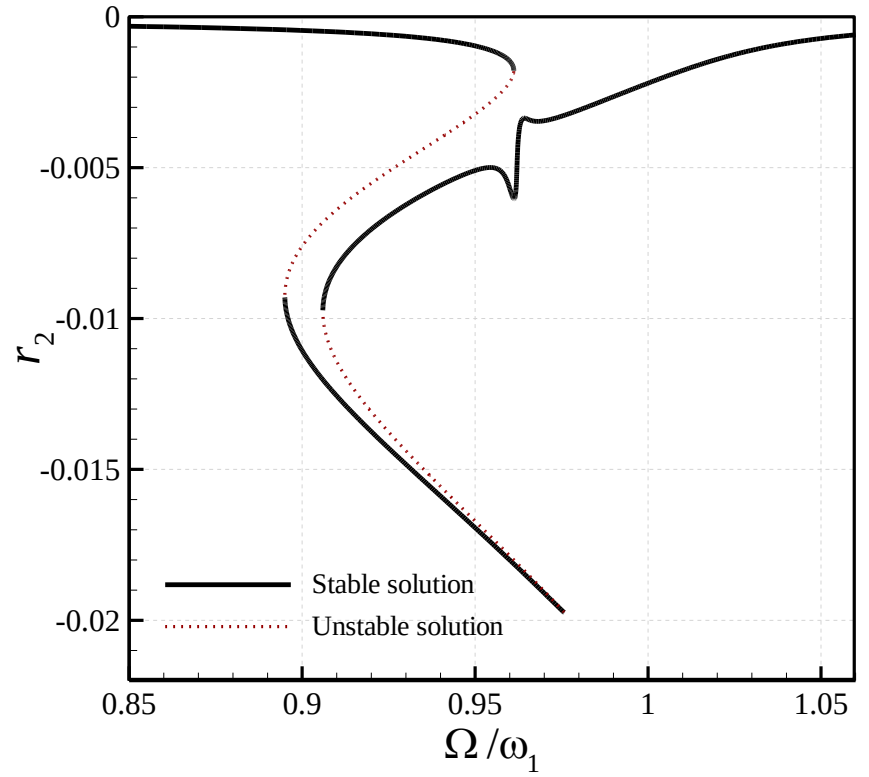

Fig. 8. Frequency-amplitude plots of the geometrically imperfect nanotube; (a-c) the maximum of q_1, q_2, and q_3, respectively; (d) the minimum of r_2 for non-zero χ_{nl} and A_0=1.5.

(a)

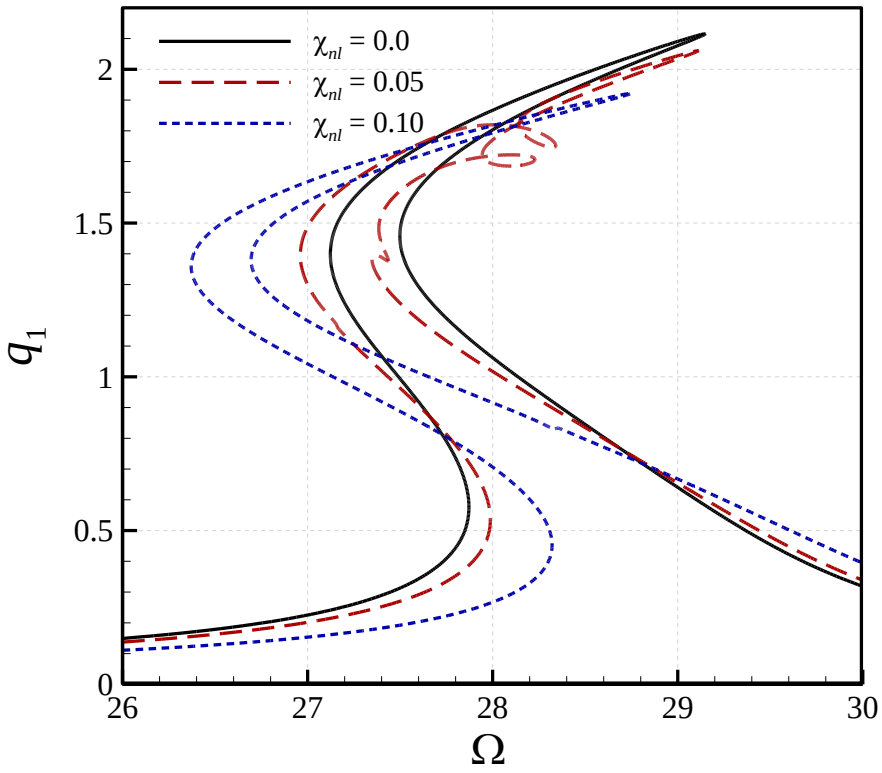
χ_{nl} = 0.0
χ_{nl} = 0.05
χ_{nl} = 0.10
q_1
Ω
0
0.5
1
1.5
2
26
27
28
29
30

(b)

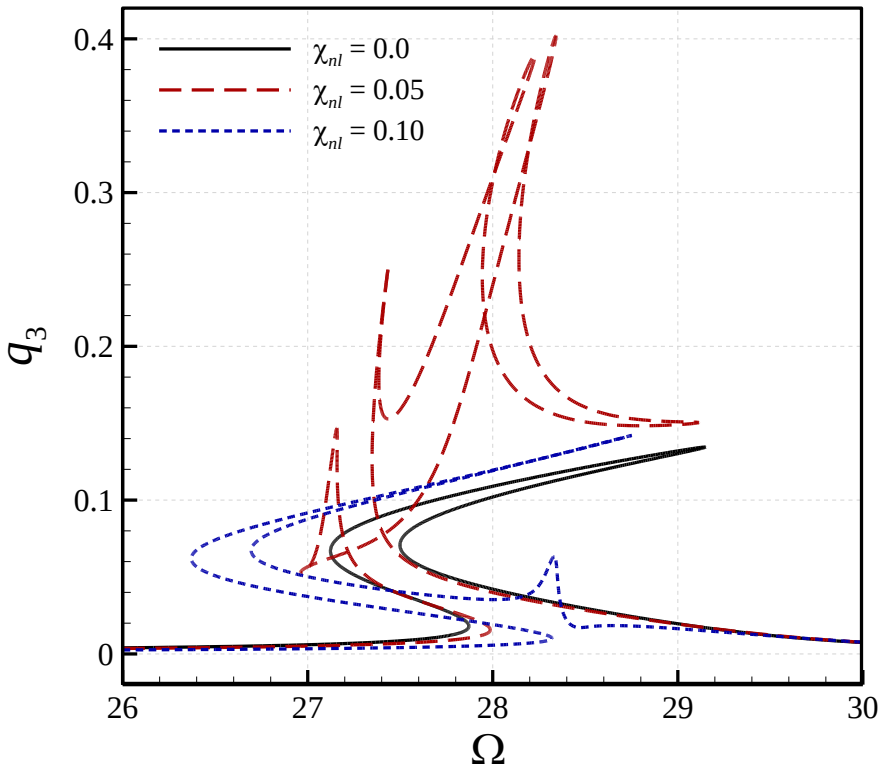
χ_{nl} = 0.0
χ_{nl} = 0.05
χ_{nl} = 0.10
q_3
Ω
0
0.1
0.2
0.3
0.4
26
27
28
29
30

(c)

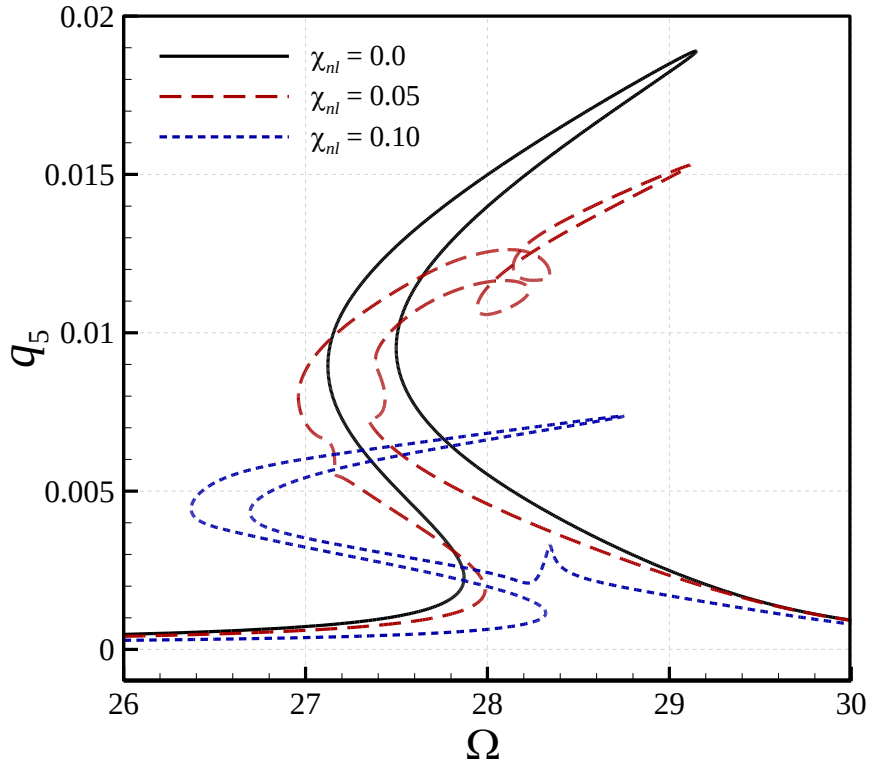

(d)

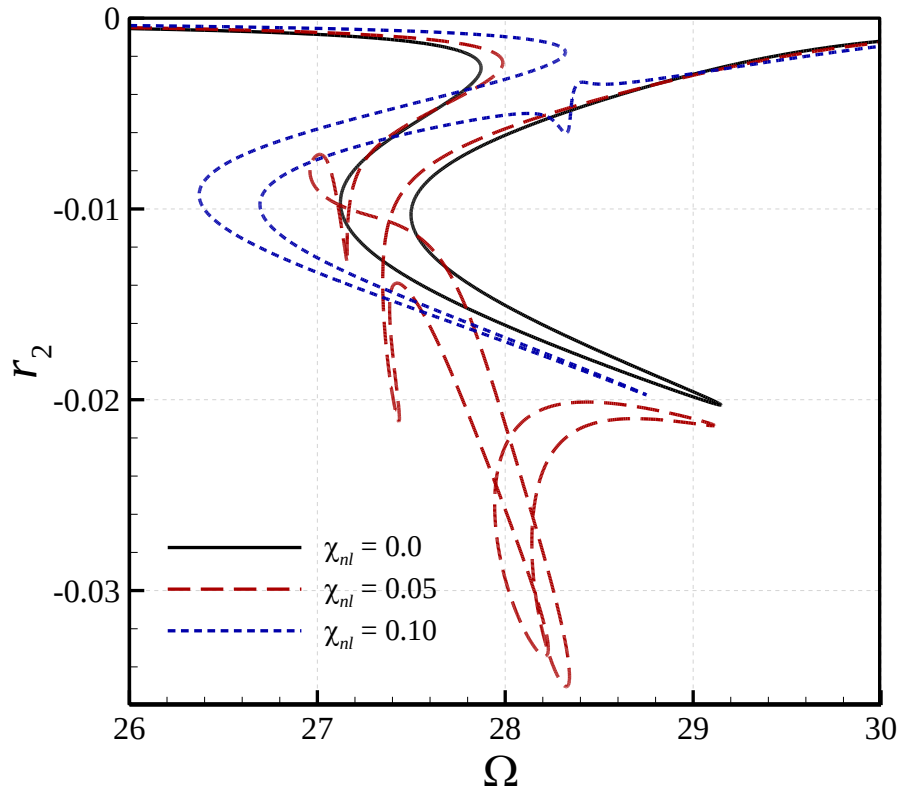

Fig. 9. Nonlocal effects on frequency-amplitude plots of the geometrically imperfect nanotube; (a-c) the maximum of q_1, q_2, and q_3, respectively; (d) the minimum of r_2 for A_0=1.5.

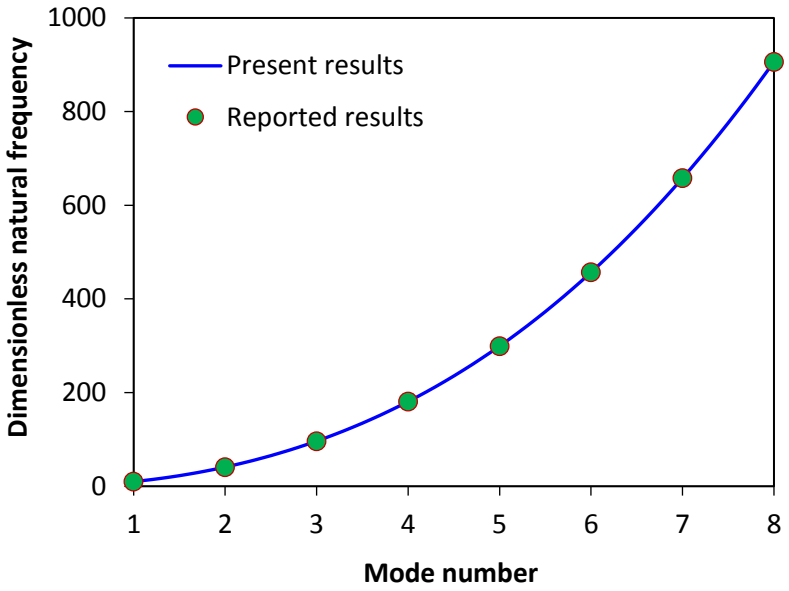

Fig. 10. Comparison of the present results with those reported in Ref. [53] for linear perfect NSGT nanobeams.